PREDITION OF TORQUE AND RADIAL FORCES IN PERMANENT MAGNET SYNCHRONOUS MACHINES USING FIELD RECONSTRUCTION METHOD

by

BANHARN SUTTHIPHORNSOMBAT

Presented to the Faculty of the Graduate School of

The University of Texas at Arlington in Partial Fulfillment

of the Requirements

for the Degree of

MASTER OF SCIENCE IN ELECTRICAL ENGINEERING

THE UNIVERSITY OF TEXAS AT ARLINGTON

MAY 2010

ACKNOWLEDGEMENTS

I would like to sincerely appreciate several people who have contributed me to get through this work. First of all, one of the most altruistic attitudes is to contribute to the wealth and growth of young generations. I wish to express respectfully my gratitude to my advisors, Dr.Babak Fahimi, for his valuable support, understanding and encouragement. His incitement kept me going throughout this thesis. I respectfully thank him for his didactic know-how about power electronics and electrical motor drives to me as well as for proof-reading the script, and for being a man of great standing both professionally and socially.

I would like to express my sincere thanks to Dr.Kambiz Alavi and Dr.Rasool Kenarangui, who were members of the committee. They offer several illustriously beneficial doctrines and comprehensive knowledge to me.

I am also grateful to members of renewable energy and vehicular technology laboratory (REVT Lab), the University of Texas at Arlington, who provided an inspiring and enjoyable working environment and many constructive discussions.

Most of all, I would like to thank my beloved family, especially my parents, who devoted love, constant support, and strong willpower to make me into what I am. I would honestly dedicate this work to be their legacy.

April 19, 2010

ABSTRACT

PREDITION OF TORQUE AND RADIAL FORCES IN PERMANENT MAGNET SYNCHRONOUS MACHINES USING FIELD RECONSTRUCTION METHOD

Banharn Sutthiphornsombat, M.S.

The University of Texas at Arlington, 2010

Supervising Professor: Dr. Babak Fahimi

Due to their high torque-to-loss ratio, permanent magnet synchronous machines (PMSM) have received increasing attention in automotive applications over the past decade. Because of this unique characteristics, many applications have utilized PMSM. In addition to high efficiency, quiet operation of the machines is desirable in automotive, naval and military applications. In order to operate at high efficiency quietly, the torque pulsation or torque ripple needs to be monitored and mitigated accurately. Magnitude of the torque ripple is influenced by the magnetic design (cogging torque) and excitation, and the pattern of ripple is affected by the machine's geometry (stator slots).

Field reconstruction method (FRM) has been presented and used in this thesis. FRM introduces the reconstruction of the electromagnetic fields due to the phase currents using basis functions and using one single magnetostatic solution from FEA.

The implementation of field reconstruction method based on finite element analysis (FRM based on FEA) is performed Matlab/simulink program. Principally, the FRM needs the three-phase stator currents and rotor position of the machine. Next, to accurately calculate torque pulsation, the tangential and normal components of magnetic field, need to be computed. As a result, FRM can correctly calculate the torque of PMSM.

In experience, the investigation shows that FRM can accurately calculate the torque pulsation or cogging torque under both balanced and unbalanced operations. Furthermore, the FRM can confirm the effect of torque ripple originated from the geometry of PMSM. In fact, a 12 stator slots PMSM was studied, and the calculation was done by FRM. The resultant torque calculated by FRM shows the accurate calculation of the torque. The experimental results show that FRM can accurately predict the torque.

TABLE OF CONTENTS

LIST OF ILLUSTRATIONS

Figure Page

CHAPTER 1

INTRODUCTION

Permanent magnet synchronous motors (PMSM) are efficiently used in industrial applications, such as automotive, assembly line, and servo applications. Not only is the PMSM easy to control, but it also has relatively higher power density. In fact, since the rotor of PMSM provides the constant field by the virtue of permanent magnet, it does not require an auxiliary source of magnetization flux. Moreover, the PMSM Can be developed using surface mounted magnets or using embedded permanent magnets.

Due to the presence of permanent magnets, the power factor and efficiency of the PMSM drives (especially in constant torque region) is expected to be higher than those of induction and switched reluctance motor drives. Other advantages of PMSM drives include absence of brushes, high torque/inertia ratio, and negligible rotor losses. These attributes make PMSM a competitive candidate in various high-performance, robotic, and servo applications. There have been a number of methods to control the performance of PMSM. For instance, field oriented control (FOC) is emphasized on fast torque response of the PMSM. Furthermore, direct torque control (DTC) is also focused on the torque response [1]-[2]. Nevertheless, in some applications, such as naval,

automotive, and submarines, PMSM drives are required to illustrate a quiet operation. This is not necessarily furnished by FOC or DTC methods.

In order to control the machines to operate quietly, several researchers have proposed analytical methods [3]-[13]. Over the past decades, the technological breakthrough of modern power electronics has been introduced and utilized to implement complex systems along with adaptive and flexible control algorithms. In order to eliminate/mitigate the acoustic noise and vibration in electric machines the origins of this phenomenon should be identified first.

Generally the majority of the vibrations within an electrical machine are originated by the virtue of the electromagnetic forces that are acting in tangential and radial directions. While radial vibration causes vibration of the stator frame in radial direction, the tangential vibration generates pulsations acting on the shaft (and components that are in tandem with the shaft) in the machine.

Torque pulsation in PMSM can be attributed to number of sources, including the geometry of the machine, unbalanced operation, non-sinusoidal distribution of the magneto-motive force, and error in feedback measurement and controls. The tangential and radial forces are dependent upon the distribution of the magnetic field in the air gap. One of the methods that are employed to analyze torque pulsation is based on finite element analysis (FEA). Nevertheless, in practice FEA is not suitable for the real time torque ripple minimization because of its inadequate computational time [5]-[6].

Several researchers have proposed methods on how to mathematically predict the electromagnetic torque in PMSM [3]-[7]. The next step is to use the calculated torque and radial forces in conjunction with an optimization method to minimize the pulsation which leads to reduction of the acoustic noise and vibration originated from electromagnetic forces acting on the stator frame [3]. The success of the noise mitigation technique, therefore, is closely related to the precision of torque and radial force calculations.

1.1 Background and Overview of Previous Works

In PMSM, torque pulsation and vibration can be attributed to a number of sources, including unbalanced excitation design of the machine, misalignment, and error of feedback measurement to control the system. To solve these problems, there are two main approaches, which are the improvement of structure of the machines and development of optimal control methodology [3], [14], [15]. The change of geometry of the machines has been the focus of many researchers in reducing cogging torque or torque pulsation in PMSM [2]. In addition, there have been problems from the unbalanced mass of rotor and misaligned installation of the machine [16]. These also contribute to the vibration. Nevertheless, changing and modification of machine's structure are not always the solution because if the machine is already built, change of the control is about the only feasible solution.

In literature [6] and [7], authors proposed the control of current waveforms to reduce the torque pulsation. Moreover, several researcher presented alternative control

techniques, such as adaptive control algorithm [8], to achieve torque pulsation minimization, and online estimated instantaneous values based on electrical subsystem variables. These techniques have been implemented in either speed or torque control loops [9]–[12].

1.2 Outline of Present Work

The present thesis can be divided into 5 chapters. In the first chapter, significance, state-of-the-art and motivations of the research are described. Sources of torque pulsation and vibration have been explored as well. Background and overview of previous works is also included.

Chapter 2 depicts the analysis and modeling of PMSM from electromechanical energy conversion point of view. The mathematical model of PMSM is also presented in this chapter.

Field reconstruction method (FRM) and force calculation are described in chapter 3. In this chapter, the concept of FRM and force calculation based on finite element analysis (FEA) has been explored. Moreover, the detail of FRM, including basis function algorithm, has also been discussed.

Chapter 4 contains the experimental results. It also compares the torque pulsations between FRM and KollMorgan programmable drive system. Sets of balanced and unbalanced loads are applied into the system at different rotor speed.

Chapter 5 concludes the experimental results.

CHAPTER 2

PERMANENT MAGNET SYNCHRONOUS MACHINES

2.1 Introduction

A permanent magnet synchronous machine is one of the most prominent electromechanical energy converters. When the PMSM is operated as a motor, it converts energy from electrical to mechanical form. On the other hand, when it is operated as a generator, it is converting the energy from mechanical to electrical form. In this chapter, Fundamentals of design, modeling and construction of the PMSM drives will be discussed. Moreover, it also focuses on force distribution Within the PMSM. This can be interpreted as energy conversion in a localized and microscopic level. This provides an insightful approach to distribution of the electromagnetic forces within PMSM.

2.2 Energy Conversion in a PMSM

According to Lorentz's force formulae a current carrying conductor that is placed in a magnetic field will experience forces. This is a major phenomenon in electric machines. As known, the relationship between flux density B and field intensity H in a magnetic circuit plays a key role in electromechanical energy conversion. The relative equation between B and H can be expressed by equation (1) and the B-H curve is also displayed in figure 2.1.

$$B = \mu \cdot H \tag{2.1}$$

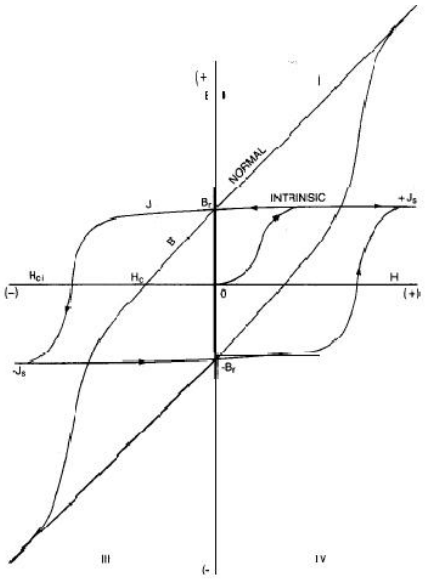

Figure 2.1 B-H Curve for a typical permanent magnet material

2.2.1. Basic Operation of a PMSM

Electric machinery may be classified according to their electrical excitation namely AC- and DC-machines. The fundamental operations of these two classes of the machine is decoupling between the armature and field excitations. The principles of operation within a PMSM can be described using eth elementary electromechanical converter shown in figure 2.2.

Figure 2.2 illustrates a singly excited actuator with two poles. The stator coil is excited by stator current, and the rotor does not contain any coil for external excitation. The role of the permanent magnet is to magnetize the core of the machine. When the

leakage into the adjacent pole with opposite polarization is negligible, and an AC-signal excitation is applied to the stator coils with a frequency corresponding to the mechanical speed of rotation, the fluxes generated due to the two sources interact to produce a resultant field. This field is non-uniform over the machine, and it is a function of magnitude of the instantaneous value of current in each phase.

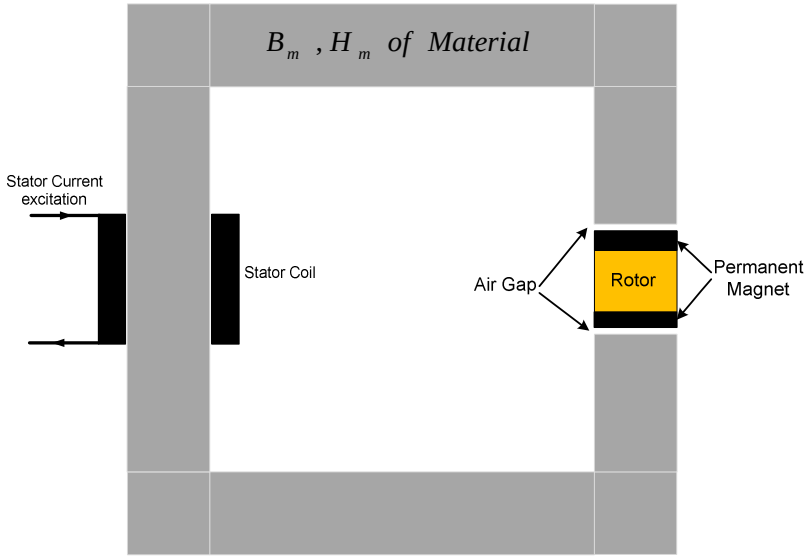

Figure 2.2 Representation of a simply single phase PMSM with stator current excitation and permanent magnet at rotor

In the same manner, in the three-phase PMSM, there are three excited stator coils, and the rotor is a permanent magnet. In this work, each phase of stator coil has 12 stator slots, and the rotor has four poles of permanent magnet. Three-phase AC-signal excitation are applied into the stator coils, and the frequency of injected AC signal is corresponding to the rotor speed of the machine as well.

Permanent magnet synchronous machines are designed to enhance the efficiency, power density, absence of brushes, torque/inertia ratio, and negligible rotor losses. These are the results of permanent magnet at rotor. The permanent magnet in rotor gives a constant field, light weight, needless of brushes, and no losses. These are why the PMSM is a competitive candidate for many high-performance and servo applications.

The PMSM can be categorized into two types. One has a sinusoidal distribution of magnetic field caused by permanent magnet. The machine is supplied with a sinusoidal excitation either current or voltage, and it generates a sinusoidal back electro-motive force (Back-EMF) which is shown in figure 2.3.

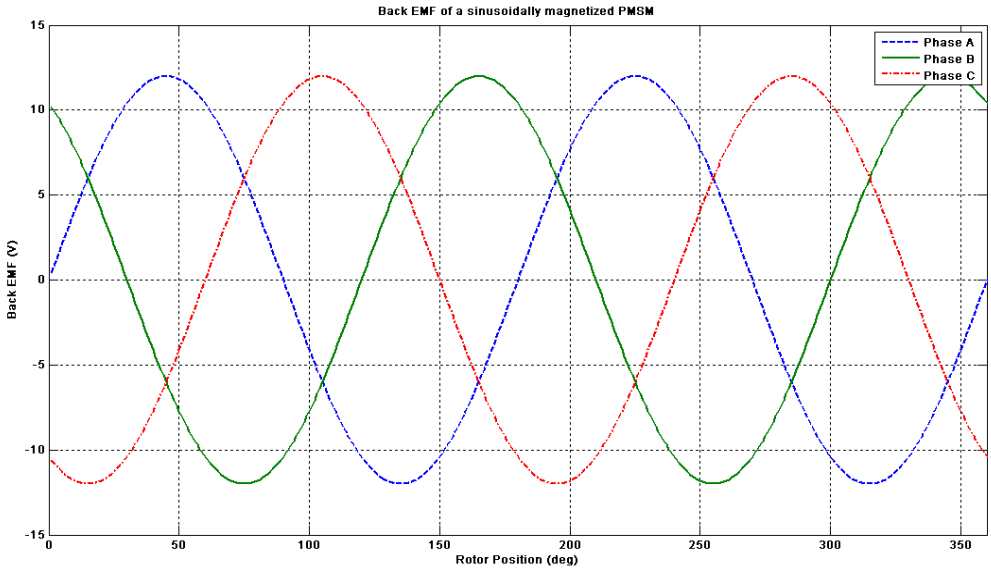

Figure 2.3 Back EMF of a PMSM with sinusoidal distribution of magnets

The other type of PMSM has a radial polarization of the permanent magnets and has a trapezoidal back-EMF as depicted in figure 2.4. This type of PMSM needs to be fed by quasi-rectangular shaped currents into the machine.

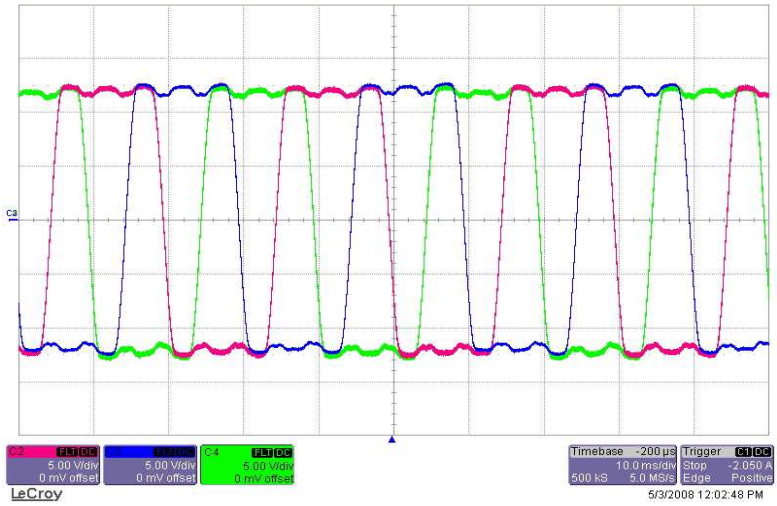

Figure 2.4 Back EMF of a PMSM with radial magnetization

The PMSM is constructed with two major parts, stator and rotor, as shown in figure 2.5.

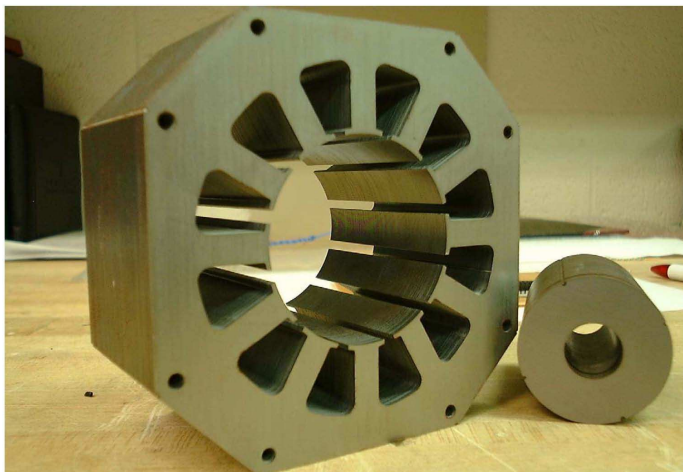

Figure 2.5 Structure of stator and rotor for 3-phase PMSM

Figure 2.5 shows a 12 stator slots and a rotor constructed with laminated iron sheets. The structure of stator and rotor is punched with laminated iron core because of reducing eddy current losses in stator and rotor. From the rotor structure, there are two different ways to place permanent magnets on the rotor. Based on placement, the PMSM can be classified into two groups. They are called surface mount permanent magnet synchronous motors (SPMSM) and interior permanent magnet synchronous motors (IPMSM). Figure 2.6 depicts the cross-section of SPMSM and IPMSM with the position of permanent magnet.

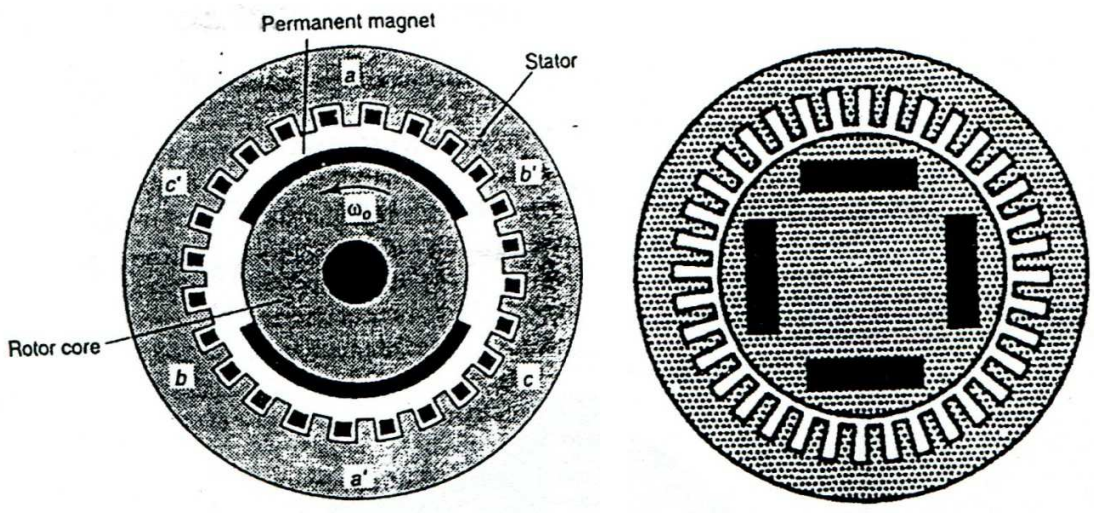

(a) (b)

Figure 2.6 Cross section of permanent magnet synchronous motor
(a) Surface mount permanent magnet synchronous motor
(b) Interior permanent magnet synchronous motor

The first group is called surface mount permanent magnet synchronous motor (SPMSM). The permanent magnet is placed on the surface of the rotor. SPMSM is easy to build owing to the ease of magnet mounting. Moreover, the configuration is usually utilized for low speed applications and low torque response. The magnetic material on the surface of the rotor affects the flux distribution in the airgap because the permeability of the permanent magnet is almost unity, which is closed to the air permeability. When the current is injected into the stator winding, the stator flux is generated and reacted with the flux from permanent magnet of the rotor. As a result, the electromagnetic torque acting on the shaft is produced. Figure 2.7 demonstrates the rotor shaft for 4-pole, 3-phase SPMSM, which has the permanent magnet mounted on the surface of the rotor.

Figure 2.7 Structure of 4-poles rotor with permanent magnet at the surface

The other group is named interior permanent magnet synchronous motor (IPMSM). IPMSM contains permanent magnets embedded inside the rotor as show in

figure 2.8. This geometric difference alters the IPMSM's characteristics. In fact, IPMSM is suitable for high speed operations. Furthermore, because of the permanent magnet mounted inside the rotor, it has more robust permeability and relatively larger magnetizing inductance since the effective airgap being low. The armature reaction effect is dominant, and therefore IPMSM is possible to be controlled in the constant-torque and the constant-power flux-weakening. Moreover, a saliency is introduced in the machine (Lq > Ld, which is discussed in section 2.3), and as a result, the torque is contributed by field as well as reluctance effect.

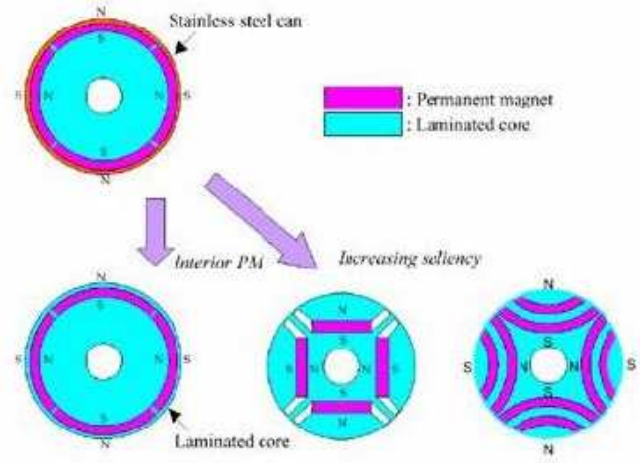

Figure 2.8 Structure of interior permanent magnet synchronous motor (IPMSM)

2.3 Modeling of PMSM

2.3.1. The definition of rotor velocity and position in PMSM

In electrical motor, there are electrical and mechanical values for rotor velocity and position. For instance, mechanical rotor position corresponds to the actual position

of the shaft during rotation. Consequently the time necessary for 360 degrees of mechanical rotation is referred to as mechanical cycle. On the other hand, an electrical cycle is the rotation of electromagnetic field around the airgap For example, figure 2.9 demonstrates a 3 phases, 4 pole permanent magnet synchronous motor. As can be seen, if the rotor shaft rotates 180 mechanical degrees (a half mechanical cycle), the electrical position of the rotor rotates 360 electrical degrees (one electrical cycle). From this statement, the relationship between electrical position and mechanical position can be concluded in equation 2.2.

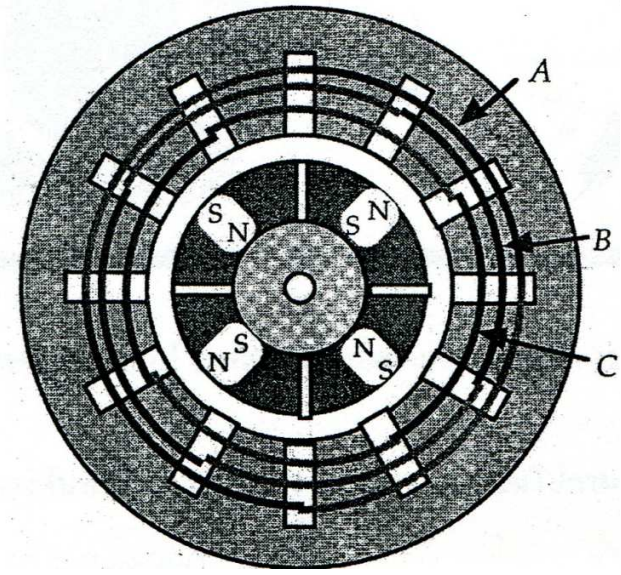

Figure 2.9 Simplified structure of 3 phases, 4 poles permanent magnet synchronous motor

$$\theta_e = \frac{P}{2} \cdot \theta_m \tag{2.2}$$

where θ_e , θ_m and P denote the electrical rotor position, the mechanical rotor position, and the number of rotor poles, respectively.

In the same manner, the rotor velocity can be represented by equation 2.3, which is based on equation 2.2 ($\omega = \frac{d}{dt}\theta$).

$$\omega_e = \frac{P}{2} \cdot \omega_m \tag{2.3}$$

where ω_e , ω_m and P denote the electrical rotor velocity, the mechanical rotor velocity, and the number of poles, respectively.

2.3.2 Electromechanical Description

PMSMs with non-sinusoidal rotor field have been held responsible for producing torque ripple on the shaft of the motor [26]. This could be a significant drawback, especially for servo applications. Over the last two decades, different methods to reduce torque ripple in permanent magnet machines have been developed. These methods can be divided into two different categories as following:

(a) Methods that are based on introducing a change in the design of the machines in order to reduce torque ripple. Many different techniques have been introduced and torque ripple can be greatly reduced at the cost of a more complex design and, thus, a more expensive machine.

(b) Methods that are based on controlling current so that the torque ripple is cancelled out. A variety of methods have evolved using different techniques to achieve the goal. In the mitigation of torque ripple, methods typically rely on a detailed knowledge of the machine. This is accomplished by schemes that

identify the parameters of the machine during startup and also during operation [25] or adaptive control of current [26].

Traditional analysis of permanent magnet synchronous machines has been based on an analytical relationship between the *q*- and *d*-axis stator current (or voltage) and the electromagnetic force created to establish motion (torque). The following two subsections introduce the electrical equivalent circuit for each phase of the PMSM, present equations for torque and also establish the significance of accurate estimation of flux linking each phase of the stator.

There are three basic components to the model of an electromechanical device - the voltage equation, the flux linkage equation and the torque equation. The equivalent circuit of the machine can be described as a series combination of the coil resistance, inductance of the winding and the back-emf due to the rotor speed and induced flux. Figure 2.10 shows this equivalent circuit.

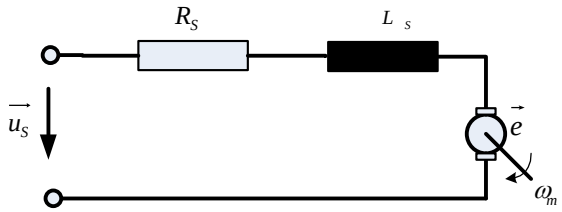

Figure 2.10 Equivalent circuit model for phase winding of the PMSM**.**

Accordingly, the voltage equation of the series circuit is defined as the algebraic sum of the ohmic drop and the rate of change of flux linkage (Faraday's law) given by equation 2.4 and it is including the effect of back motional EMF.

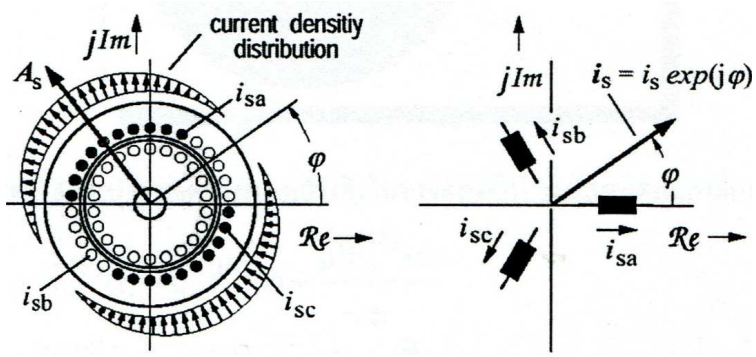

Figure 2.11 The simplified PMSM in term of 3-phase space vectors

Figure 2.11 shows the state space model of a 3-phase system. In order to simplify the 3-phase system to 2-phase system, Park's transformation to put everything on the rotor is applied into the stator voltage, current, and flux linkage vectors as shown in equation (2.4) – (2.6), and they are on the stator reference frame.

$$\vec{u}_s^{(S)}(t) = \frac{2}{3}(u_a(t) + a \cdot u_b(t) + a^2 \cdot u_c(t)) = U_\alpha + jU_\beta \quad (2.4)$$

$$\vec{i}_s^{(S)}(t) = \frac{2}{3}(i_a(t) + a \cdot i_b(t) + a^2 \cdot i_c(t)) = I_\alpha + jI_\beta \quad (2.5)$$

$$\vec{\psi}_s^{(S)}(t) = \frac{2}{3}(\psi_a(t) + a \cdot \psi_b(t) + a^2 \cdot \psi_c(t)) = \Psi_\alpha + j\Psi_\beta \quad (2.6)$$

Where a denotes an unit vector and the argument is equal to $e^{j\frac{2\pi}{3}}$. In addition, $u\,, i\,, and\, \psi$ denote phase voltage, current, and flux linkage, respectively. In those equations, the superscript "(S)" denotes the stator reference frame. Therefore, the next step is to transform the stator reference frame to the rotor reference frame. In order to easily depict the transformation, figure 2.12 is shown the space vectors in stator and

rotor reference frame in PMSM. From the figure 2.12 and the equivalent circuit model of PMSM, the stator voltage is shown in equation (2.7).

$$\vec{u}_s^{(S)}(t) = R_s \cdot \vec{i}_s^{(S)}(t) + \frac{d}{dt}\vec{\psi}_s^{(S)}(t) \quad (2.7)$$

where; $$\vec{\psi}_s^{(S)}(t) = L_s \cdot \vec{i}_s^{(S)}(t) + \Psi_m \cdot e^{j\theta_e} \quad (2.8)$$

Then; $$\vec{u}_s^{(S)}(t) = R_s \cdot \vec{i}_s^{(S)}(t) + L_s \cdot \frac{d}{dt}\vec{i}_s^{(S)}(t) + j\omega_e \Psi_m e^{j\theta_e} \quad (2.9)$$

$R_s, L_s, \omega_e, \theta_e, and\ \Psi_m$ denote the stator winding resistance, stator winding inductance, electrical angle position of rotor, electrical angle velocity of rotor, and constant flux rotor from permanent magnet, respectively.

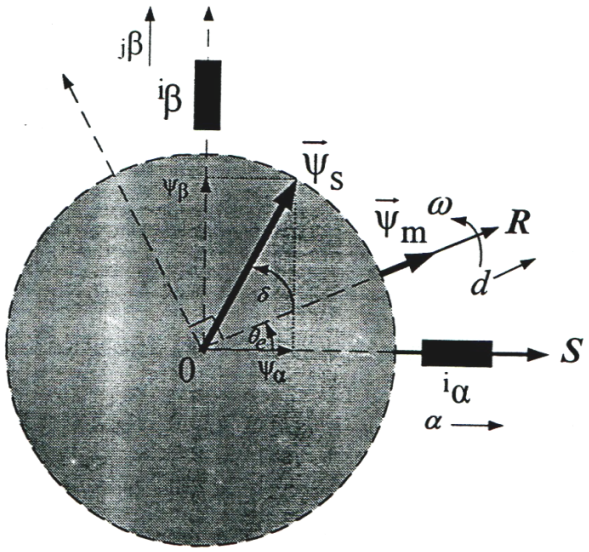

Figure 2.12 The space vector of stator and rotor reference frame in PMSM
[The superscript "(R)" denotes the rotor reference frame (d-q axis).]

As shown in figure 2.12, the relationship between stator and rotor reference frame is as:

$$\vec{u}_s^{(R)}(t) = \vec{u}_s^{(S)}(t) \cdot e^{-j\theta_e} \tag{2.10}$$

$$\vec{i}_s^{(R)}(t) = \vec{i}_s^{(S)}(t) \cdot e^{-j\theta_e} \tag{2.11}$$

Therefore, the equation (2.9) can be rewritten in rotor reference frame as equation (2.12).

$$\vec{u}_s^{(R)}(t) = R_s \cdot \vec{i}_s^{(R)}(t) + L_s \cdot \frac{d}{dt}\vec{i}_s^{(R)}(t) + j\omega_e L_s \vec{i}_s^{(R)}(t) + j\omega_e \Psi_{\mathrm{m}} \tag{2.12}$$

From equation (2.12), it can be divided into real and imaginary term as shown in equation (2.13) – (2.15).

$$\vec{u}_s^{(R)}(t) = U_d + jU_q \tag{2.13}$$

$$U_d = R_s \cdot i_d + L_s \cdot \frac{d}{dt} i_d - L_s \omega_e i_q \tag{2.14}$$

$$U_q = R_s \cdot i_q + L_s \cdot \frac{d}{dt} i_q - L_s \omega_e i_d + \omega_e \Psi_m \tag{2.15}$$

The output mechanical torque generated 'm_M' in a synchronous machine is related to the mechanical speed 'ω_m' at the steady state as given by equation (2.16).

$$m_M = \frac{U_a I_a + U_b I_b + U_c I_c}{\omega_e} \tag{2.16}$$

Further, the equation for motion of PMSM is given by equation (2.17).

$$m_M - m_L = J\frac{d}{dt}\omega_m(t) + B\omega_m \tag{2.17}$$

Where m_M , m_L , J , $and\ B$ denote mechanical torque (generated), mechanical load torque, moment of inertia, and friction, respectively.

Moreover, the equation for electrical torque in a PMSM at the steady state can be written in term of magnetizing flux and stator phase currents on the rotor reference frame as shown in equation (2.18).

$$mM = \frac{3}{2}\frac{P}{2}\left[\Psi_m I_q + \left(L_d - L_q\right) I_q I_d\right] \tag{2.18}$$

As discussed in section 2.2.1, the SPMSM is a non-salient machine ($L_d = L_q$), but the IPMSM is a magnetically salient machines$\left(L_q > L_d\right)$. Therefore, if the machine is a surface mount permanent magnet synchronous motor, the electrical torque is finally shown in equation (3.11).

$$m_M = \frac{3}{2}\frac{P}{2}\Psi_m I_q \tag{2.19}$$

In the equation (2.17), Ignoring the dynamic friction of the system, the block diagram of SPMSM on the rotor reference frame can be shown in figure 2.13 by using equation (2.4) - (3.11) [24].

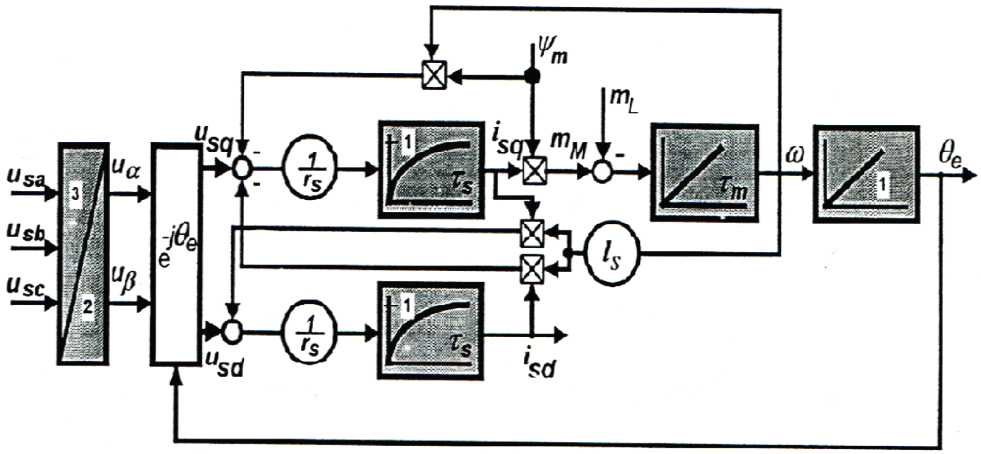

Figure 2.13 Block diagram of SPMSM on the rotor reference frame
[τ_S is the electrical time constant, and it is equal to $\frac{L_s}{R_s}$]
[τ_m is the mechanical time constant, and it is equal to 1/J]

2.4 Force and Torque Distribution in PMSM

The acoustic noise and vibration in PMSM are caused by two major categories of force, namely tangential and radial. While radial vibration causes vibration of the stator frame along in radial direction, the tangential vibration generates pulsations acting on the shaft (and components that are in tandem with the shaft) in the PMSM. In order to clarify the concept of vibration and force, those radial and tangential forces need to be discussed.

Radial forces cause the radial vibration of the machines. Consequently, these forces are the unwanted byproducts of the electromechanical energy conversion. In fact, the direction of the radial forces is perpendicular to that of the rotation of the machine. Its direction is in the normal direction (90^o apart from tangential) of the rotor and

producing unwanted radial vibration in the stator frame. These forces are local vector quantities that have different effects on different parts of the machine. To the contrary, the tangential component of force in terms of torque is mostly responsible for the motion and is a component that needs to be controlled precisely. However, when the machine is operated, it cannot avoid having the radial forces acting on the rotor and stator frames. Using Maxwell stress method distribution of the radial and tangential force densities in the airgap of the machine can be expressed as equations 2.20 and 2.21, respectively.

$$f_n = \frac{1}{2 \cdot \mu_o} \cdot (B_n^2 - B_t^2) \tag{2.20}$$

$$f_t = \frac{1}{\mu_o} \cdot (B_n \cdot B_t) \tag{2.21}$$

Where $f_n, f_t, B_n, B_t,$ and μ_0 denote normal and tangential component of the force density in airgap, normal component of flux density, tangential component of flux density, and absolute permeability, respectively.

The electromagnetic torque of PMSM is generated by the tangential forces acting on the rotor. In fact, the tangential force is dependent upon the distribution of the magnetic field in the airgap. The tangential forces are also produced on the stator poles and cause unwanted vibrations in the stator frame. Therefore, mitigation of acoustic noise and vibration includes influencing not only the normal, but also the tangential forces. These forces are generating the electromagnetic torque on the rotor and

tangential vibration of the stator frame. However, some significant conditions need to be considered, regarding force distribution in electromagnetic devices.

First of all, the magnetic field density and magnetic energy inside the unsaturated ferromagnetic material are very small. Therefore, the force contributions from these components are very small. Moreover, the relative permeability of permanent magnet is very close to unity. The force distribution in the air and PM are therefore identical for the same position if the points that are probed are close.

Next, radial forces throughout any component exhibit different magnitudes at different points. Therefore, compensation cannot always be based on the average values measured in the machine. Local effects need to be taken into account. In addition, local saturation is observed at pole tips owing to a large concentration of flux. This causes a much larger force at the tip of the stator poles than the rest of the pole. At the surface of a material with high permeability, the tangential component of flux density is almost equal to zero, and the normal force density almost entirely depends on normal component of flux density. On the other hand, the tangential component of force is almost zero at the surface of high permeable material for the same reason.

Finally, from an energy's point of view, almost all the energy exchange happens at the iron-air interface as the system moves [20]. In fact, a region with highest energy density is replaced by a region with almost zero energy density, as such the highest rate of energy change with incremental displacement happens at the interface of iron and air, and thus almost all the force as the normal component produces on the surface of the

iron toward the air.

2.4.1 Fields and Forces at the interface between two materials

In this section, the analysis of fields and forces between two materials acting inside the machines are considered. The theory of continuity [22] plays a key role in explaining the distribution of tangential and normal field and force components. The field and force components can be considered in two parts, including tangential (the same direction with rotating direction) and normal (90^o apart from rotation direction). The field density and field intensity at the interface between materials having different permeability are given in accordance with continuity theorem in equations 2.22 and 2.23. However, zero surface current densities at the surface of the stator pole−airgap interface−needs to be assumed.

$$B_{n,M19} = B_{n,air} \tag{2.22}$$

$$H_{t,air} = H_{t,M19} \tag{2.23}$$

Equation 2.23 given above can be expresses in terms of permeability as

$$\begin{aligned} \frac{B_{t,air}}{\mu_{air}} &= \frac{B_{t,M19}}{\mu_{M19}} \\ B_{t,M19} &= B_{t,air}\,\mu_{r,M19} \end{aligned} \tag{2.24}$$

From equation 2.24, we see that the tangential component of field density at the interface of two materials with different permeability is not continuous. Since the permeability of M-19 is of the order of 10^5, the tangential field density inside the iron is

much greater than that present in the air outside it. To assess the influence of these components on the force generated at that surface, we consider the tangential component of force given by the equation

$$f_t = H_t B_n \tag{2.25}$$

$$f_{t,air} = \frac{1}{\mu_{air}} B_{t,air} B_{n,air} \tag{2.26}$$

$$f_{t,M19} = \frac{1}{\mu_{M19}} B_{t,M19} B_{n,M19} \tag{2.27}$$

Using the expressions for $B_{n,\ M19}$ and $B_{t,\ M19}$ from equations 2.22 and 2.24 respectively in equation 2.28, tangential force component in M-19 is given by

$$f_{t,M19} = \frac{1}{\mu_0} B_{t,air} B_{n,air} \tag{2.28}$$

At the air- M19 interface, the tangential component of flux density in the air is almost zero. Therefore, with this information, it can be observed from equations 2.26 and 2.28 that the magnitude of tangential component of force inside and outside the iron is very negligible when it is compared to the normal components. In the iron- air interface, it can be seen that the tangential force present inside the iron is almost zero. On the other hand, the normal component of force at the interface is given as following:

$$f_{n,air} = \frac{1}{2\mu_0}(B_{n,air}^2 - B_{t,air}^2) \approx \frac{1}{2\mu_0} B_{n,air}^2 \tag{2.29}$$

$$f_{n,M19} = \frac{1}{2\mu_0}(B_{n,M19}^2 - B_{t,M19}^2) \approx \frac{1}{2\mu_0} B_{n,M19}^2 \tag{2.30}$$

This is a very large value since the magnitude of B_n is unchanged in either case. Therefore, the investigation of the field a component at the interface indicates that tangential component of the field in the air-side of the interface is significantly smaller than the normal component. Therefore, it can be said that the forces on a conducting body with no surface current density are produced on the surface of iron as the normal force component. In fact, the normal force component is directed toward the air, and it is higher where the surface flux density is higher. If this normal force happens to be in the same direction of rotating motion, it is viewed as a useful result of the electromechanical energy conversion. Otherwise, it is viewed as a troublesome by product that causes noise, vibration, and deformation. The higher the normal surface force in the direction of movement and lower on other directions, the more efficient energy conversion process is resulted.

2.5 PMSM Drive Setup

There can be divided the PMSM drive setup into four major parts, including motor, generator, loads, and torque meter parts. Figure 2.14 shows the experimental setup.

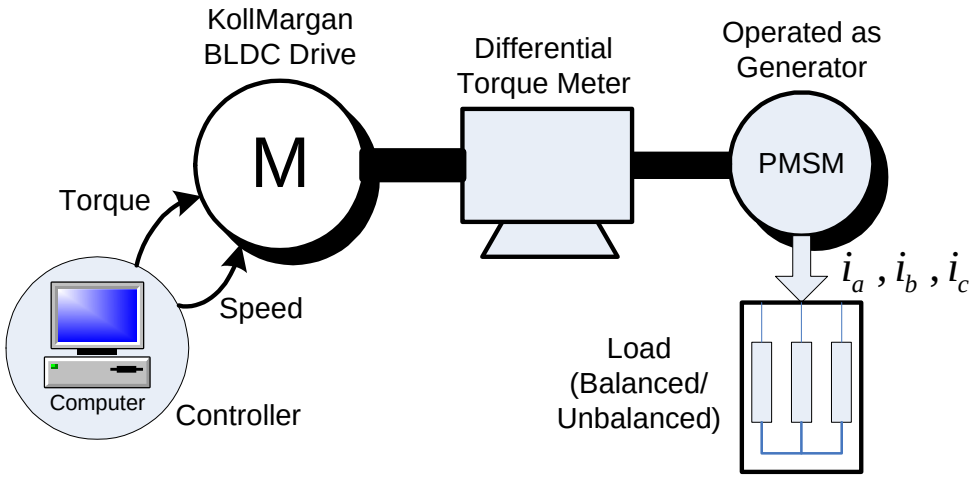

Figure 2.14 System demonstrating the experimental setup

In this work, PMSM is driven by a brushless direct current motor drive system (BLDC Drive). The BLDC system is controlled by programmable controls, named as KollMorgan drive system. This work is setup to utilize the KollMorgan drive system to operate in “motoring mode.” Figure 2.15 shows the KollMorgan system that is used in the laboratory.

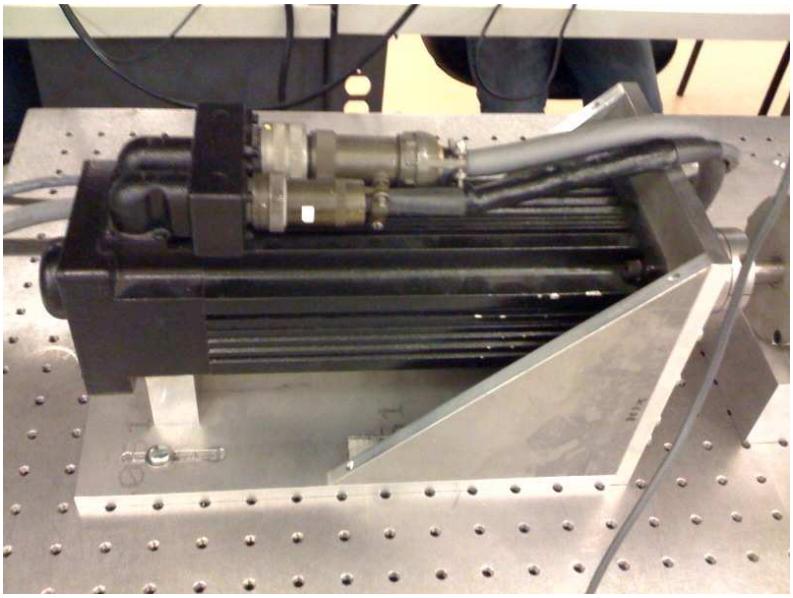

Figure 2.15 KollMorgan system in REVT laboratory

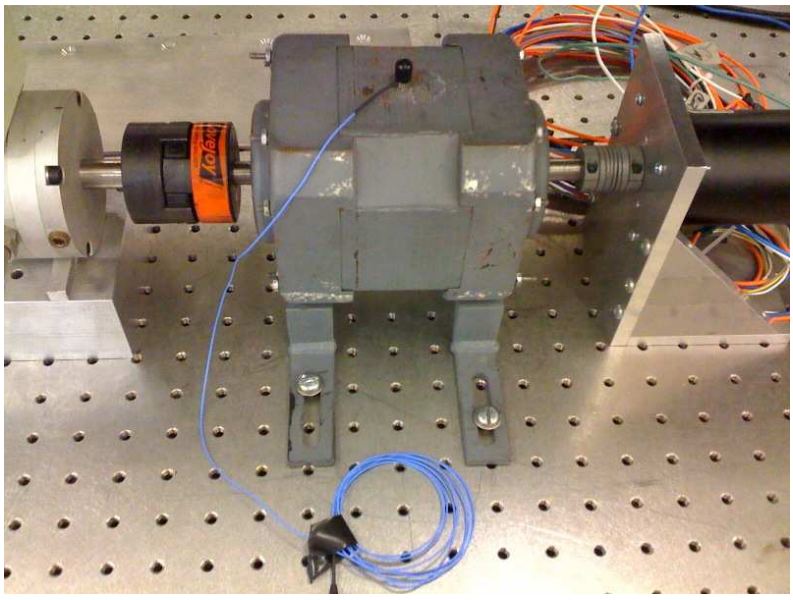

Figure 2.16 The 3-phase, 4 poles permanent magnet synchronous motor

The next part is the PMSM. The PMSM is operated in “generating mode.” BLDC is programmed to drive the PMSM, and the balanced and unbalanced loads are applied to the 3-phase voltage terminals of PMSM. Figure 2.16 shows the PMSM that is employed in the experimental setup.

In this setup, resistive loads are applied to the PMSM’s terminals. There are both balanced and unbalanced loads to demonstrate the cogging torque both balanced and unbalanced three-phase currents. The three-phase current profiles is utilized in the field reconstruction method (FRM) in MATLAB program to compute the torque. Then the FRM’s torque calculation is compared with the torque from BLDC. This will be discussed in chapter 4. Figure 2.17 demonstrates the resistant loads that are used in this experimental setup.

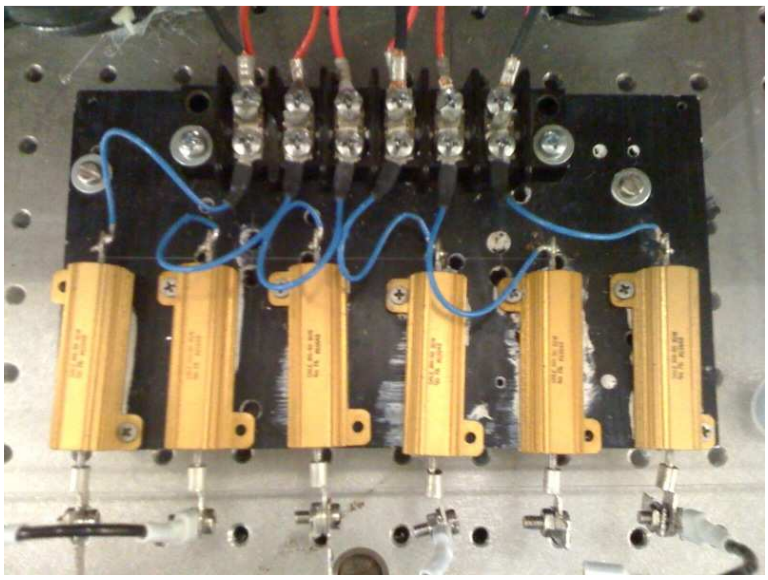

Figure 2.17 Demonstrating resistant loads in experimental setup

The other part of the system is a torque meter. This torque meter is a differential torque meter, which means at the steady state the output of the torque meter is equal to zero. Figure 2.18 shows the torque meter in this setup.

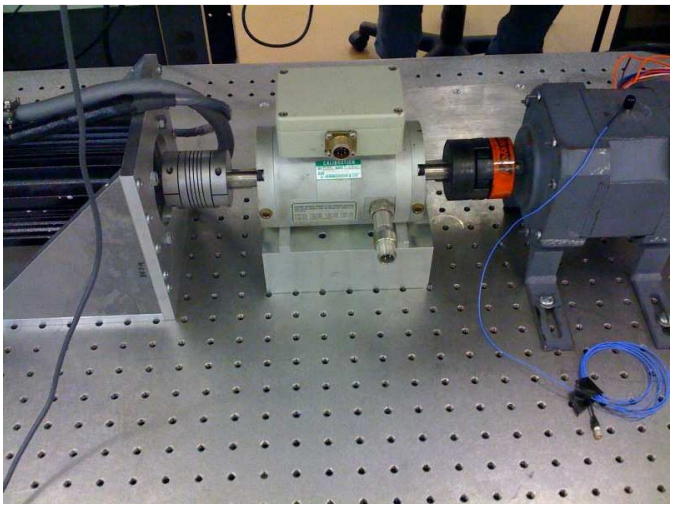

Figure 2.18 Differential torque meter

CHAPTER 3

FORCE CALCULATION AND FIELD RECONSTRUCTION METHOD

The force calculation of PMSM has been proposed on several levels. For instance, field oriented control technique (FOC) for PMSM is based on the assumption of a purely sinusoidal back electromotive force (back-EMF). In this technique, the three-phase currents are transformed from 3-axis to 2-axis system on stator reference frame. Thereto, 2-axis currents are metamorphosed from stator reference frame to rotor reference frame at steady state, which are DC terms. This method gives a good result of force calculation. Nevertheless, it is time consuming [20]-[21].

Another technique is direct torque control technique (DTC) [2]. Based on this idea, the force calculation is computed on stator reference frame, and the 2-axis currents have still been used. However, the problem is stator fluxes, including direct axis and quadrature axis components of flux, in AC terms. These stator fluxes are included an integral part of calculation, which is added to previous error in every single calculation. Consequently, the stator fluxes are draft until they are saturated.

As a result, many researchers have proposed several methods to calculate the force [17]-[19]. In addition, the method is computational time and precision. Remarkably, numerical methods are seemingly suitable for force computation [20]-[21].

3.1 Force Calculations

The calculations of electromagnetic force can be viewed as the main part of simulating the electromechanical energy conversion process. So far many numerical methods and formulations for force calculation have been proposed, such as finite element analysis (FEA), finite difference method (FDM), magnetic equivalent circuit (MEC), Fourier series method (FSM), and some global or local variation and mapping techniques. They all are based on approximations of the electromagnetic fields and stored magnetic energy in the machine. All of the above methods, because of flexibility, ease of modeling and post processing, finite element analysis, FEA, has evidently been a good candidate and employed to efficiently compute the electromagnetic force.

Along those lines, electromagnetic force can be computed by the virtue of the Maxwell Stress Tensor (MST), which is one of the numerical methods and based on FEA. Necessary calculations of electromagnetic forces acting on the stator and rotor are presented in the literature [18]-[19]. In order to perform the analysis, the following assumptions have been setup:

- Surface mounted magnets on the rotor of the PMSM are uniformly magnetized.
- Influence of eddy and hysteresis currents is negligible.
- The stator is slot-less with m independent stator phases distributed around a uniform airgap.
- Operation under saturation is not allowed.

The majority of the energy conversion takes place in the airgap. The tangential and radial components of force density in the airgap can be expressed using equation (3.1)-(3.2), and they also represent the basis for an investigation of the force production within the machine.

$$f_t = \frac{1}{\mu_0}(B_n B_t) \tag{3.1}$$

$$f_n = \frac{1}{2\mu_0}(B_n^2 - B_t^2) \tag{3.2}$$

where $f_n, f_t, B_n, B_t \; and \; \mu_0$ denote normal and tangential component of the force density in airgap, normal and tangential component of flux density, and absolute permeability respectively.

3.2 Field Reconstruction Method (FRM)

In the electromechanical energy conversion (EMEC), it is very important to obtain the flux density distribution, so is the field reconstruction method (FRM). Figure 3.1 shows a block diagram representation of field reconstruction method [20]-[21].

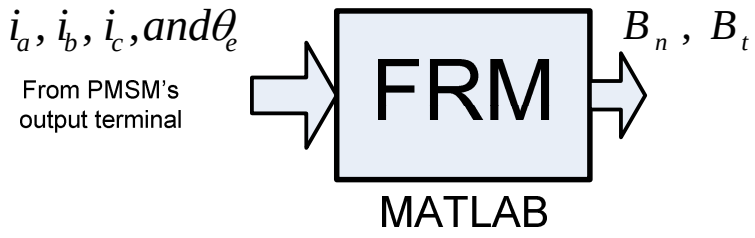

Figure 3.1 Demonstration of field reconstruction method

As seen in figure 3.1, FRM needsthe input of three-phase current profiles and rotor position in order to calculate the flux density distribution.

In order to efficiently design FRM and the machine, simulation is first needed to be done before designing the machine. In fact, the finite element analysis (FEA) is utilized in the simulation. In this particular approach, commercially available software-Magnet® by Infolytica was used. For a complete simulation of the 3-phase permanent magnet synchronous machine, there are four basic inputs. They include three phase currents and mechanical speed of the rotor. The resultant normal and tangential components of flux density in the airgap for any rotor position were obtained from the FEA solution. Corresponding force densities were calculated using Maxwell Stress Tensor method as described in equations (3.1) and (3.2). For obtaining the solution, a 2-dimensional cross section was used, as shown in figure 3.2.Figure 3.3 shows the 3-dimensional finite element model of the PMSM used for the modeling.

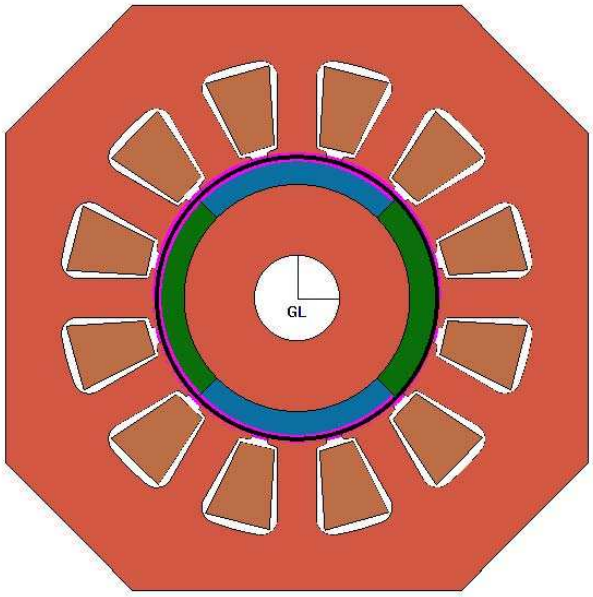

Figure 3.2 Representation of 2-Dimensional model of the PM machine used for field reconstruction.

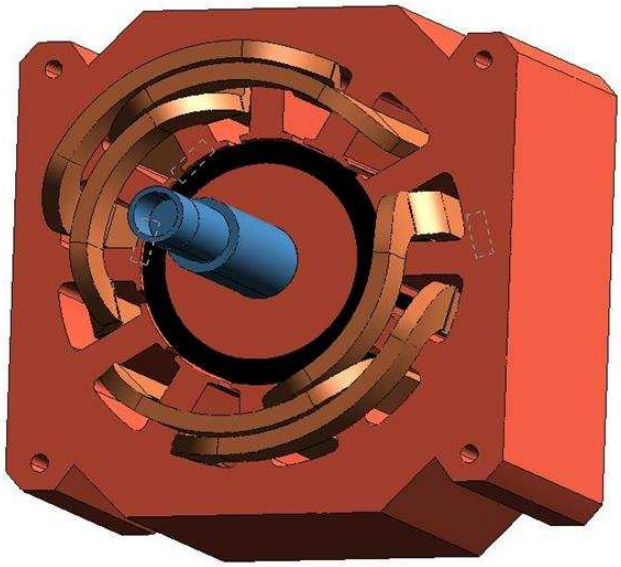

Figure 3.3 Demonstration of 3-Dimensional model of the PM machine modeled using Finite Element Analysis.

The majority of energy conversion takes place in the airgap as shown in figure 3.4. A field reconstruction method (FRM) is proposed to compute the electromagnetic torque and radial forces of PMSM. The FRM utilizes the three phase current profile and rotor position, as shown in figure 3.4, to calculate radial and tangential component of the force density and the flux density. Furthermore, FRM can predict torque ripple which is affected by geometry of the machine. Stator slots play a central role in the profile torque ripple when there is no stator excitation, known as cogging torque.

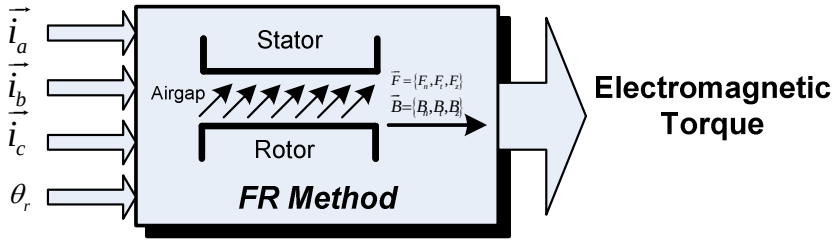

Figure 3.4 Block diagram of field reconstruction method

As can be noted from figure 3.4, using an appropriate integration contour around the stator and rotor, the actual force acting at each surface can be computed by integrating the force density components over the respective surface area as follows:

$$F_t = \oint_S \vec{f_t} dS \tag{3.3}$$

$$F_n = l \oint_0^{2\pi} r f_n d\phi_s \tag{3.4}$$

where $s, l, r\ and\ \phi_s$ represent surface area of integration, stack length of the machine (along the Z-direction), radius of the integrating contour, and angle component in cylindrical system of coordinates respectively.

Using equation (3.3)-(3.4), the electromagnetic torque can be calculated as shown in equation (3.5). As a result, these computations can be used to mitigate torque pulsation and the vibration in the stator frame.

$$T = \oint_S \left(\vec{r} \times \overrightarrow{f_t}\right) \cdot \overrightarrow{d_s} \tag{3.5}$$

Figure 3.5 illustrates the distribution of the magnetic flux density in a 3-phase PMSM due to three phases' excitation of the stator winding.

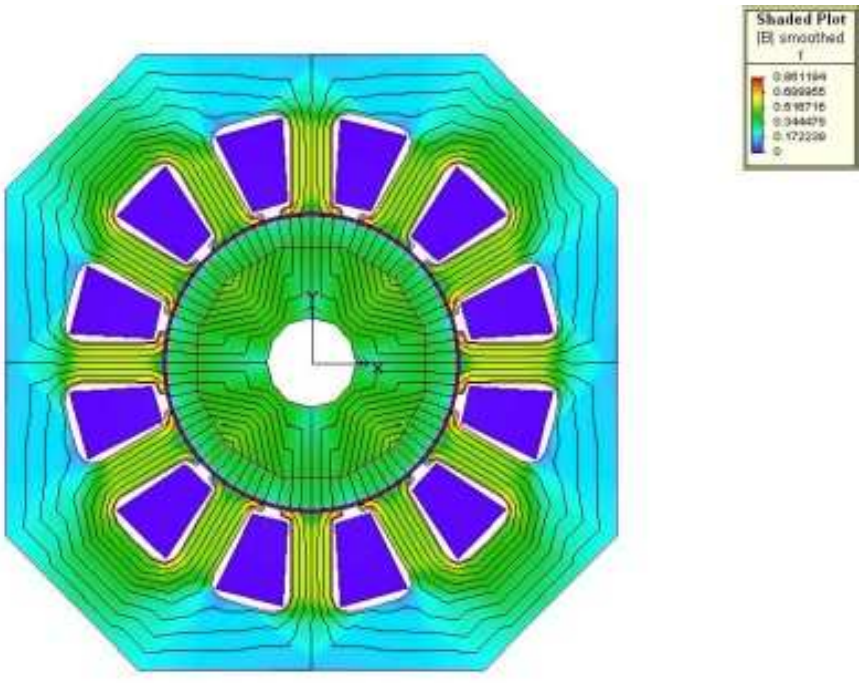

Figure 3.5 Distribution of magnetic flux density in a 3-phase PMSM

It is shown in figure 3.5 that each conductor on the stator contributes to the tangential and radial components of the flux density in the airgap. Any change in the geometry within PMSM can alter the tangential and components of the flux density that are constituted by a conductor located at ϕ_{sk} as shown in equation (3.6).

$$B_{t,k} = B_t(i_k) \cdot h_t(\phi_s - \phi_{sk}) \qquad ; 0 \leq \theta_r \leq \frac{2\pi}{P}$$

$$B_{n,k} = B_n(i_k) \cdot h_n(\phi_s - \phi_{sk}) \tag{3.6}$$

where $P, B_t, B_n, h_t \; and \; h_n$ denote number of magnetic pole pairs, scaling function representing the dependency of the tangential and radial flux density upon the current magnitude, and impact of the geometry (one conductor) respectively. Also, ϕ_{sk} represents the location of the k^{th} conductor carrying a current of i_k.

The resultant tangential and radial components of the flux density in the airgap for any given rotor position can be expressed by using superposition (including the contributions from the permanent magnets) theory and a truncated generalized Fourier series as shown in equation (3.7)-(3.8). These expressions portray an elegant illustration of the separation between factors influenced by the structure of the machines $(h_t \; and \; h_n)$ and external excitation$\left(B_{t,k} \; and \; B_{n,k}\right)$.

$$B_t(\phi_s, i_1, \dots, i_m) = B_{t,pm} + \sum_{k=1}^{m} B_{t,k}(i_k) \cdot h_t(\phi_s - \phi_{sk}) \tag{3.7}$$

$$B_n(\phi_s, i_1, \dots, i_m) = B_{n,pm} + \sum_{k=1}^{m} B_{n,k}(i_k) \cdot h_n(\phi_s - \phi_{sk}) \tag{3.8}$$

Equation (3.1) and (3.2) can therefore be rewritten by using the tangential and radial components of the force densities as follows:

$$f_t(\phi_s, i_1, \dots, i_m) = \frac{1}{\mu_0}\{B_t(\phi_s, i_1, \dots, i_m) \cdot B_n(\phi_s, i_1, \dots, i_m)\} \tag{3.9}$$

$$f_n(\phi_s, i_1, \dots, i_m) = \frac{1}{2\mu_0}\{B_n^2(\phi_s, i_1, \dots, i_m) - B_t^2(\phi_s, i_1, \dots, i_m)\} \tag{3.10}$$

In the same manner, equation (3.3) and (3.4) can also be rewritten to calculate the force density over the outer surface of a cylinder, which is located in the middle of the airgap, for each rotor position as shown in equation (3.11)-(3.12).

$$F_t(\theta_r) = P \cdot L \cdot R \int_0^{\frac{2\pi}{P}} f_t(\phi_s, i_1, \dots, i_m) d\phi_s \tag{3.11}$$

$$F_n(\theta_r) = P \cdot L \cdot R \int_0^{\frac{2\pi}{P}} f_n(\phi_s, i_1, \dots, i_m) d\phi_s \tag{3.12}$$

where $\theta, L, and\ R$ denote rotor position, stack length of the machines and radius of the integration surface respectively.

Seemingly, FRM contains key functions in equation (3.7) and (3.8), $h_t\ and\ h_n$, which are known as the basis functions. The basis functions have played a significant role in the formulation of the field reconstruction method. In equation (3.13)-(3.14), under unsaturated condition, FRM can calculate the distribution of field and force for at any given position due to stator currents when the pattern of excitation is known, and basis functions are identified. Also, the contributions of the permanent magnets will be adjusted for the new rotor position.

$$B_{t,k}(i_k) = B_t \cdot i_k \tag{3.13}$$

$$B_{n,k}(i_k) = B_n \cdot i_k \tag{3.14}$$

From equations (3.13) and (3.14), if the pattern of stator current excitation is known, and flux density distribution is also calculated from the basis functions, which are identified. As a result, equations (3.7) through (3.9) can be identified the distribution of field/force for any given position. It must be noted that the contribution of the permanent magnets are assumed as given. The basis functions h_t and h_n are an unsaturated slot-less and have characteristics as following:

- h_t has an even symmetry with respect to φ_s
- h_n has an odd symmetry with respect to φ_s.
- Periodic with respect to φ_s,

Since the rotor has constant field from permanent magnet (without rotor excitation), the resultant tangential force is, therefore, an odd function resulting in zero average torque at every given point. Nevertheless, the radial forces exist even without any magnetic source on the rotor. Figure 3.6 shows the tangential and normal components of field density in the PM machine without load.

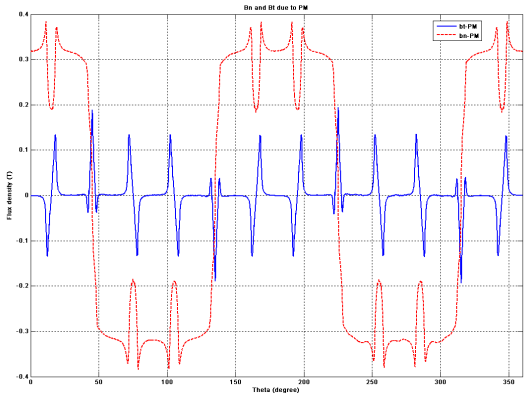

Figure 3.6 Tangential and radial flux densities in airgap generated by permanent magnets

It can also be seen that radial component of flux density in a PMSM is primarily dominated by the field of the permanent magnet. Moreover, the normal component of force density yields a nonzero average and dominated by the normal component of the flux density even though it is without applying the stator current. Therefore, radial forces, which are viewed as byproduct in electromechanical energy conversion process, are significantly larger than their tangential counterparts. It is also important to note that the tangential component of the flux density in the PMSM does not have a continuous profile and only appears at distinct positions where the stator/rotor coils are located. Integration of the tangential component of force density yields a zero average in the absence of excitation, which indicates that there is not motion when no excitation is applied.

From the above assumption, it must be noted that due to the periodic nature of the basis functions, they can be expanded by using a Fourier series, i.e.:

$$h_t(\phi_S) = \ h_{0t} \ + \ \sum_{k=1}^{M} h_{kt} \cos(k\phi_s) \tag{3.15}$$

$$h_n(\phi_S) = \ h_{0n} \ + \ \sum_{k=1}^{M} h_{kn} \sin(k\phi_{s)} \tag{3.16}$$

Where M denotes the selected truncation point that would provide satisfactory precision. In the presence of saturation, the coefficients of the above series expansion depend upon current.

In the simulation, since there is only one source of MMF in the machine during the calculation of basis functions, the amount of time taken by FEA to compute this “one-shot-result” is significantly lower than the time required for the simulation of the

complete system. Consequently, in practice FEA may not be suitable for the real time torque ripple minimization because it is time consuming [20]. This advantage may outstandingly prove that FRM is faster than FEA in real time control and more suitable. It goes on to say that this method is not just for the reconstruction of sinusoidal excitations. Since the current applied for the basis function is 1A, force calculation in the machine for various optimized waveforms becomes extremely simple.

3.3 Basis Functions of Field Reconstruction Method

As known in section 3.2, the characterization of the “basis functions” is a key function of field reconstruction method. As expressed in figure 3.7, the algorithm of field reconstruction involves a flow chart of calculation and a meticulous analysis of magnetic field distribution throughout the machine. In order to achieve this objective, unit dc current is applied to one of the phases and the resultant flux distribution is recorded. Using the inherent symmetry of the machine, this distribution can be rotated in space to establish the effect of current in each conductor of the machine. Finally, the field density distribution is obtained from the cumulative effect of current through the stator windings, and the permanent magnets gives the overall estimate of flux over the entire machine.

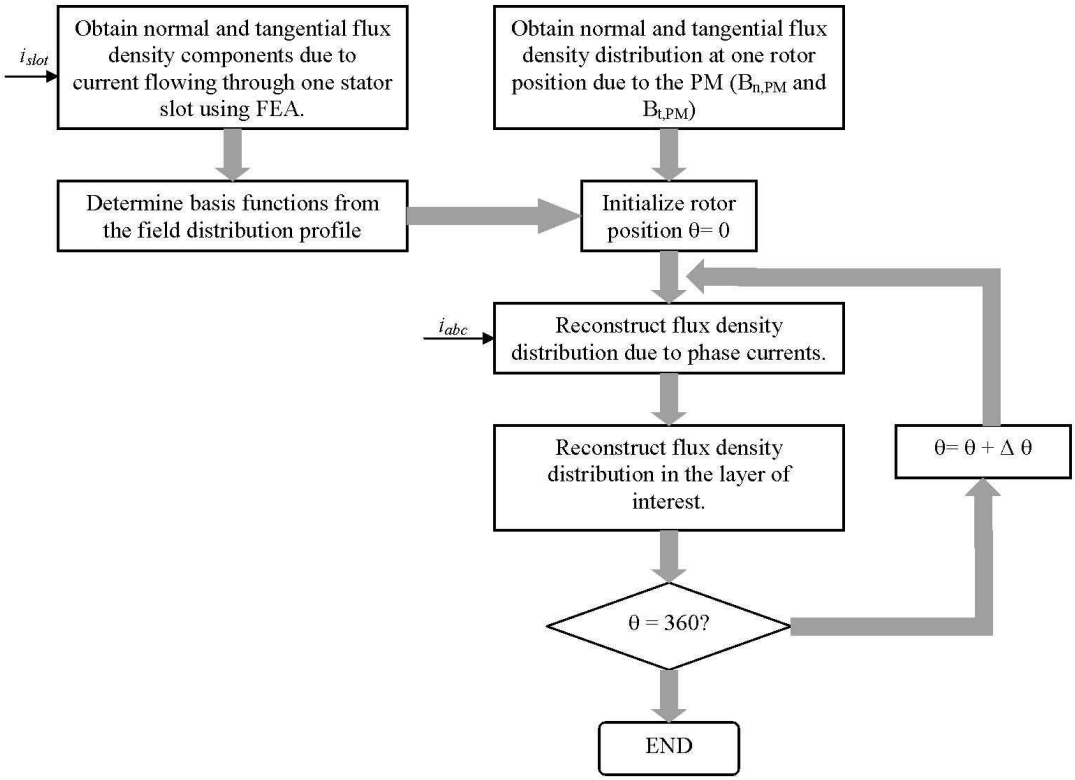

Figure 3.7 Demonstration of flow chart for field reconstruction method.

CHAPTER 4

EXPERIMENTAL RESULTS

In many applications, such as naval, automotive, and military, there are several requirements of operation. In fact, quiet and torque pulsation free (radial and tangential vibration) are desired. One of the major causes that generate sound, acoustic noise and vibration is torque pulsation. In addition, magnitude and frequency of the torque ripple is influenced by the magnetic design (cogging torque), geometry of the machine (number of stator slots), and excitation. In this work, a 1-hp, 3-phase, 4 poles, 12 stator slots PMSM has been used for simulation and experimental verification. In the simulation, the Matlab/simulink program is used to calculate the torque using FRM. In the experiment, PMSM is operated in generating mode by using a fully controllable BLDC drive system as shown in figure 2.14. Then sets of balanced and unbalanced loads are connected to the terminals of PMSM. The 3-phase load currents is measured and used in the field reconstruction program in Matlab/simulink program.

4.1 Permanent Magnet Synchronous Motor

It is important to note that the surface mounted permanent magnets are radially magnetized. Consequently, back-EMF of this machine is trapezoidal. The first experiment that has been done is to test the PMSM, and the easiest way to accomplish

this is to Run the PMSM with no stator current at a fixed speed and measure the back-EMF. In the simulation of this PMSM, FEA was used, and the magnitude of back-EMF voltage from the machine is about 12.4 volts at the speed of 1000 rpm. Figure 4.1 shows the result of back-EMF from FEA. In fact, the back-EMF is the trapezoidal waveform, and it has the magnitude of 12.4 volts. In case of comparison with an actual PMSM, figure 4.2 to figure 4.4 are the results of back-EMF at different speeds. In figure 4.2, the corresponding experimental measurement shows a measurement of back-EMF of 12.4 volts.

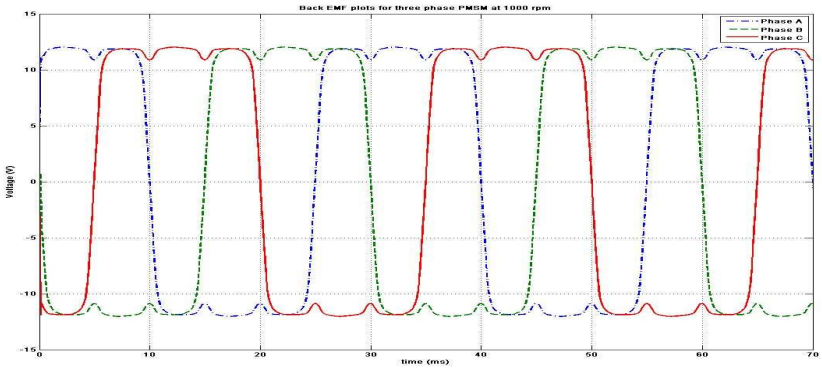

Figure 4.1 Back-EMF of PMSM at 1000 rpm from FEA

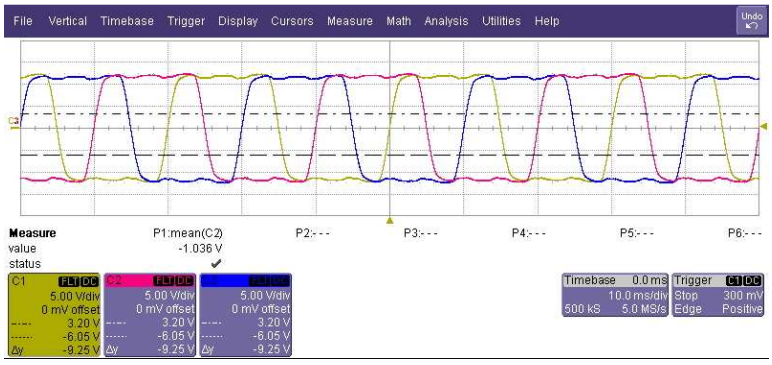

Figure 4.2 Back-EMF of PMSM at 1000 rpm from PMSM

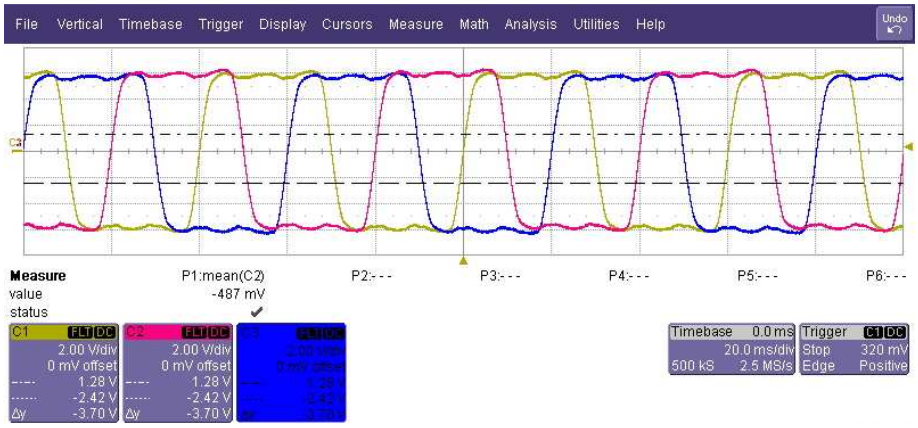

Figure 4.3 Back-EMF of PMSM 500 rpm from PMSM

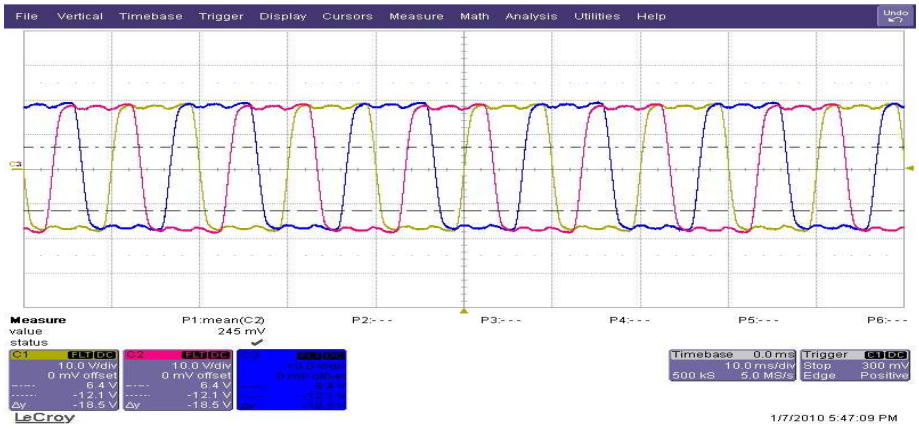

Figure 4.4 Back-EMF of PMSM 1500 rpm from PMSM

4.2 Prediction of Electromagnetic Torque

The experimental system may be divided into two main parts, which are PMSM (operating in generating mode) and KollMorgan drive (operating in motoring mode and acting as a prime mover). When The three phase terminals of the PMSM is connected to

the sets of balanced and unbalanced load, the recorded three-phase current is injected into the FRM in Matlab/simulink in order to calculate the torque of PMSM. Then the torque of PMSM is compared with the torque of the prime mover. This comparison demonstrates an a excellent match in terms of frequency and magnitude of the average torque. At steady state it is expected that the inline torque meter will show a zero average torque.

The electromagnetic torque of PMSM is computed by supplying the three-current current profiles and rotor position into Matlab/simulink program However, calculation of the torque stemming from the prime mover need to be done separately. In fact, the torque needs to be computed in Excel program by using three-phase stator current profiles, and then the currents are transformed into the rotor reference frame. As known, the quadrature axis current on the rotor reference frame Is linearly proportional to the torque of the machine, and the direct axis current on the rotor reference frame creates the magnetizing flux. As a result, after the quadrature axis current is calculated, the current value has to be calibrated into the unit of torque (Nm).

4.2.1 Calculation of quadrature axis current on rotor reference frame

In order to calculate the quadrature axis current on the rotor reference frame, the three-phase current profiles of KollMorgan must be measured, and they are on the stator reference frame. Therefore, three-phase system has to be simplified to two-phase

system by the use of Clarke's transformation. Figure 4.5 shows the three-phase current system.

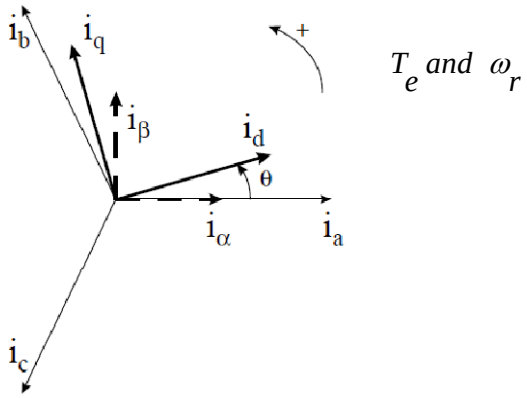

Figure 4.5 Three-phase current vectors on stator reference frame (α-β axis)

The transformation equation can be expressed as

$$f_{\alpha\beta o} = K_s \cdot f_{abcs} \tag{4.1}$$

where f represents either voltage, current, flux linkage, or electric charge, and

$$K_S = \frac{2}{3} \cdot \begin{bmatrix} \cos\theta_e & \cos\left(\theta_e - \frac{2\pi}{3}\right) & \cos\left(\theta_e - \frac{4\pi}{3}\right) \\ \sin\theta_e & \sin\left(\theta_e - \frac{2\pi}{3}\right) & \sin\left(\theta_e - \frac{4\pi}{3}\right) \\ \frac{1}{2} & \frac{1}{2} & \frac{1}{2} \end{bmatrix}$$

Then the three-phase stator current of PMSM can be transformed into two-phase system on stator reference frame as:

$$\begin{bmatrix} i_\alpha \\ i_\beta \\ i_o \end{bmatrix} = K_S \cdot \begin{bmatrix} i_a \\ i_b \\ i_c \end{bmatrix} \tag{4.2}$$

Now the three-phase system is transformed to two-phase system. The next step would be a transformation from stator reference frame to rotor reference frame, so called Park's transformation. This calculation requires a vector rotation angle into mathematical model to follow the rotor reference frame attached to the rotor flux.

The formula that is used to calculate and transform stator reference frame to rotor reference frame is shown as:

$$\begin{bmatrix} i_d \\ i_q \end{bmatrix} = \begin{bmatrix} \cos\theta_r & \sin\theta_r \\ -\sin\theta_r & \cos\theta_r \end{bmatrix} \cdot \begin{bmatrix} i_\alpha \\ i_\beta \end{bmatrix} \tag{4.3}$$

where θ_r is the rotor angle position.

4.3 Simulation and Experimental Results

There are sets of balanced and unbalanced loads at different speeds of rotor.

4.3.1 Operation under balanced loads condition

Figure 4.6 shows the three-phase balanced current of PMSM that is supplied to the loads at 167 rpm.

Figure 4.6 Three-phase current supplied to the load of PMSM at 167 rpm

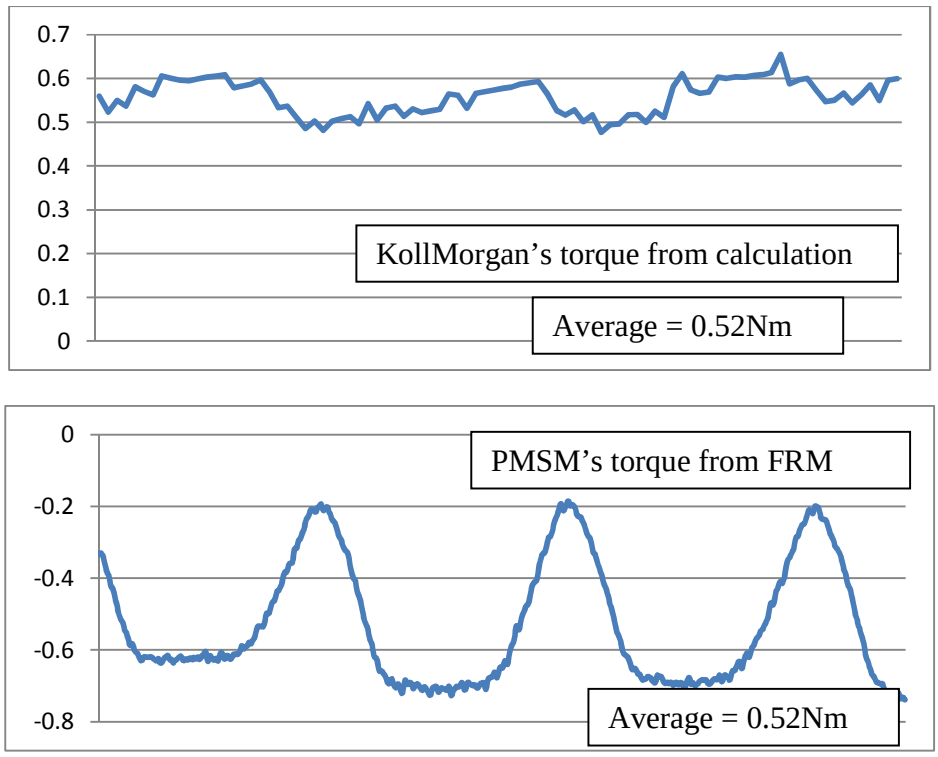

Figure 4.7 Comparative results of torque between KollMorgan and PMSM using FRM at 167 rpm under balanced load condition

Figure 4.7 shows the torque between prime mover and PMSM. The PMSM's torque is the results of a half cycle of three-phase stator current. This is because of the limitation of sampling data of FRM in Matlab/simulink program that limits the sampling of 10kH_z from the captured data to be injected into the FRM program. That is why FRM can only compute 3 cycles of torque. This result is matched with the targeted PMSM, which has 12 stator slots. Moreover, the results between KollMorgan and FRM are matched in both the average torque and the frequency.

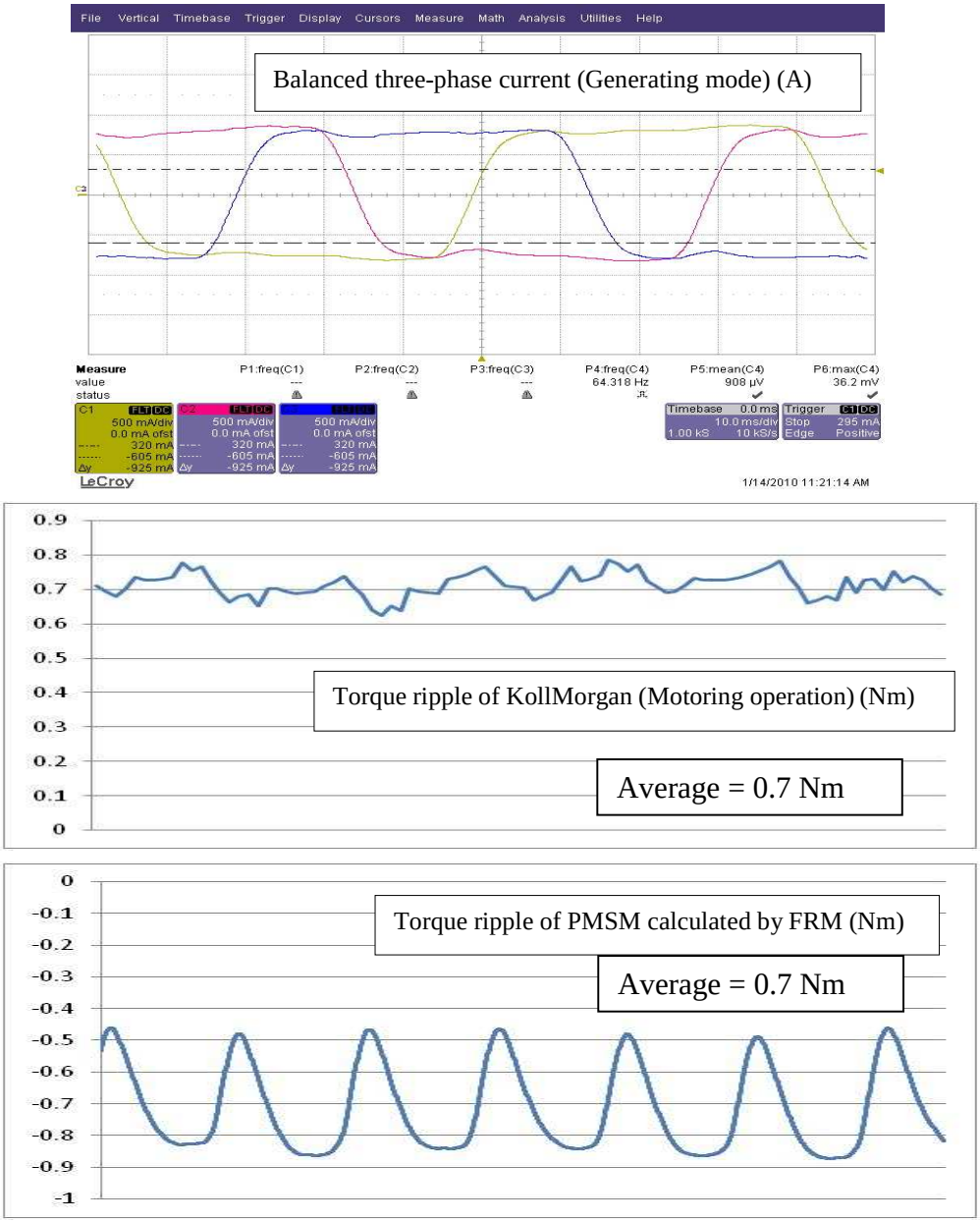

Figure 4.8 Comparative results of torque between KollMorgan and PMSM using FRM at 334 rpm under balanced load condition

Figure 4.8 shows an operation of PMSM at 334 rpm under balanced load condition. A cycle of three-phase stator current of PMSM is injected into FRM program to calculate the electromagnetic torque. Evidently, there are 6 periods of torque in one period of current, which means there are 12 stator slots. More significantly, the algebraic summation of PM's torque and KollMorgan's torque is approximately equal to zero Nm.

4.3.2 Operation under unbalanced loads condition

Figure 4.9 and 4.10 shows an unbalanced three-phase current of PMSM operating in generating mode, and the PMSM is run at 1000 rpm. The measured current has three electrical cycles. As a result, the torque pulsation will have 36 pulses due to the structure of PMSM (12 stator slot).

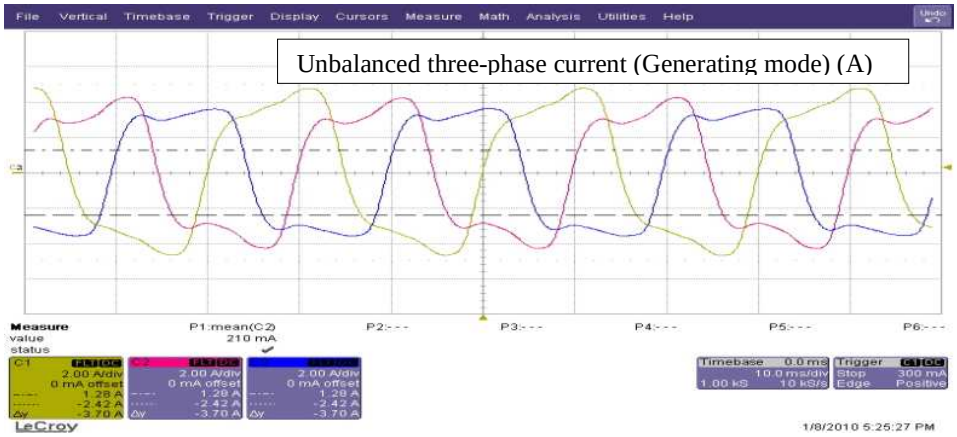

Figure 4.9 Unbalanced three-phase current of PMSM at 1000 rpm

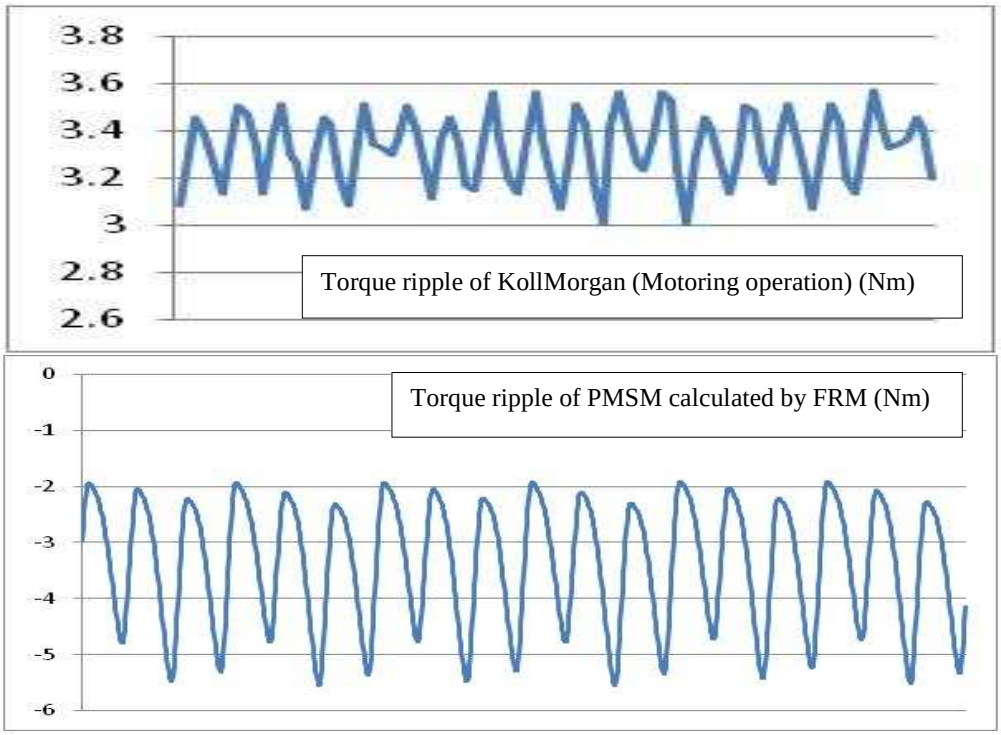

Figure 4.10 Comparative results of torque between KollMorgan and PMSM using FRM at 1000 rpm under unbalanced load condition

CHAPTER 5

CONCLUSIONS

In this research, a field reconstruction method (FRM) has been introduced and implemented on Matlab/simulink program. In case of a real time vibration and acoustic noise cancellation, the torque pulsations have to be calculated and predicted correctly.

Field reconstruction method has been presented for calculation of torque ripple. The FRM allows for the reconstruction of the electromagnetic fields due to the phase currents using basis functions that are obtained using a few snapshots of the magnetic field distribution. To accurately calculate torque, the tangential and normal components of magnetic field, need to be computed. As a result, FRM can correctly calculate the torque of PMSM.

In experiment, the investigation shows that FRM can accurately calculate the torque pulsation or cogging torque under both balanced and unbalanced operations when compared with BLDC's torque pulsation. Furthermore, the FRM can confirm the effect of torque ripple due to the geometry of PMSM. In fact, a 12 stator slots PMSM was studied, and the calculation was done by FRM. The resultant cogging torque calculated by FRM shows the accurate calculation of the torque which is affected by stator slot geometry.

Field reconstruction method is a new numerical technique for analysis and design of a PMSM. This technique is suitable with a real-time control because it consume less calculating time than FEA. Also, FRM combines ideas from electromechanical energy conversion, signal reconstruction, and pattern recognition in order to control and develop the machine efficiently.

APPENDIX A

EXPERIMENTAL TESTBED AND THE PMSM

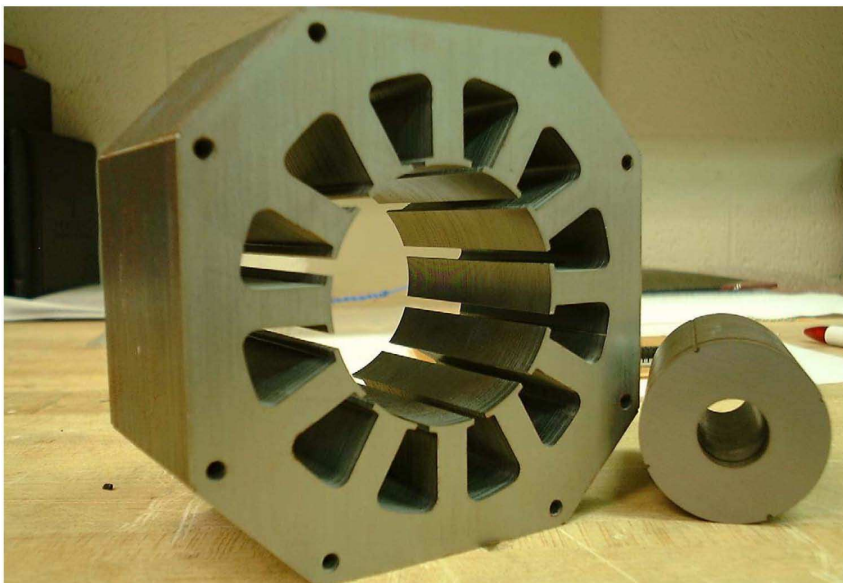

Laminated stator and permanent magnet rotor

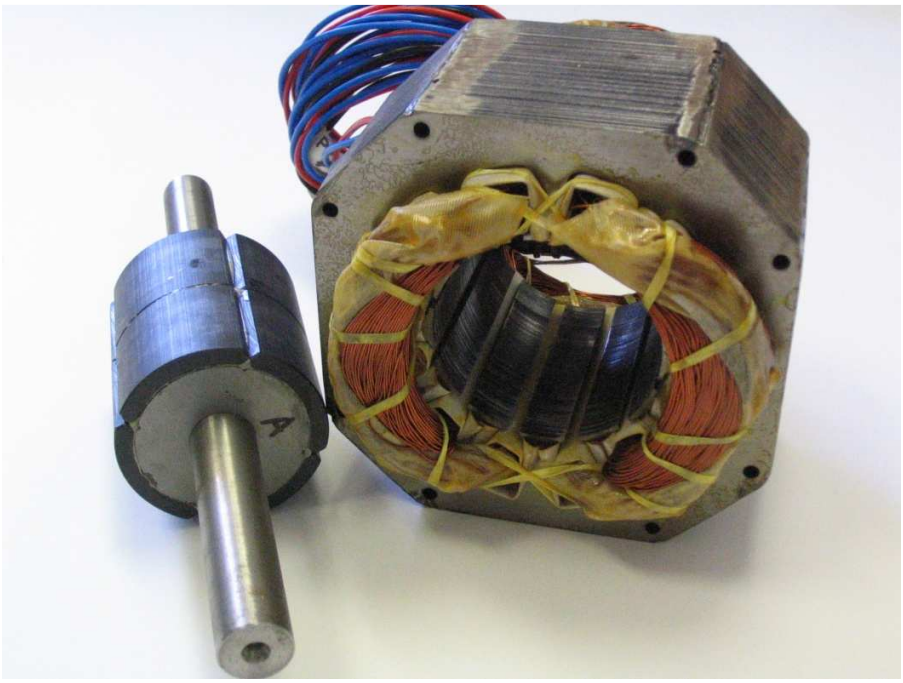

A 4 poles, 12 stator slots PMSM after winding

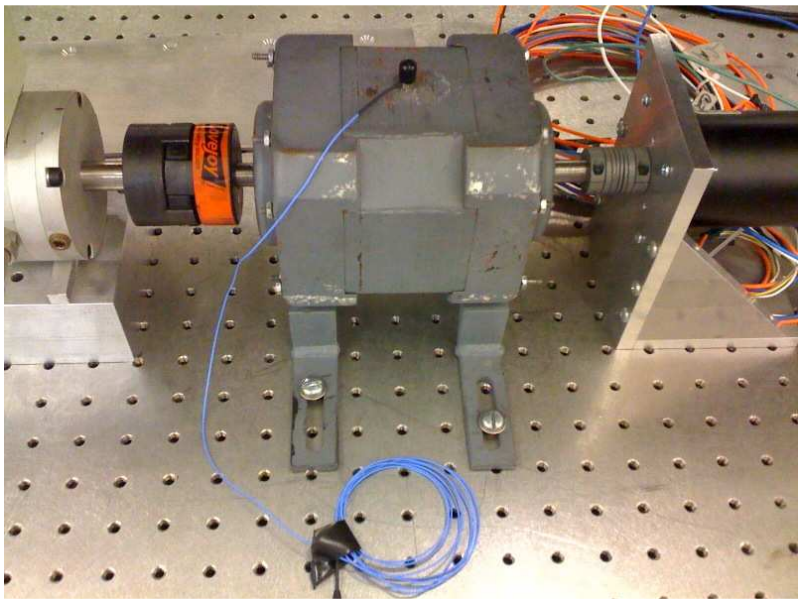

The permanent magnet synchronous motor

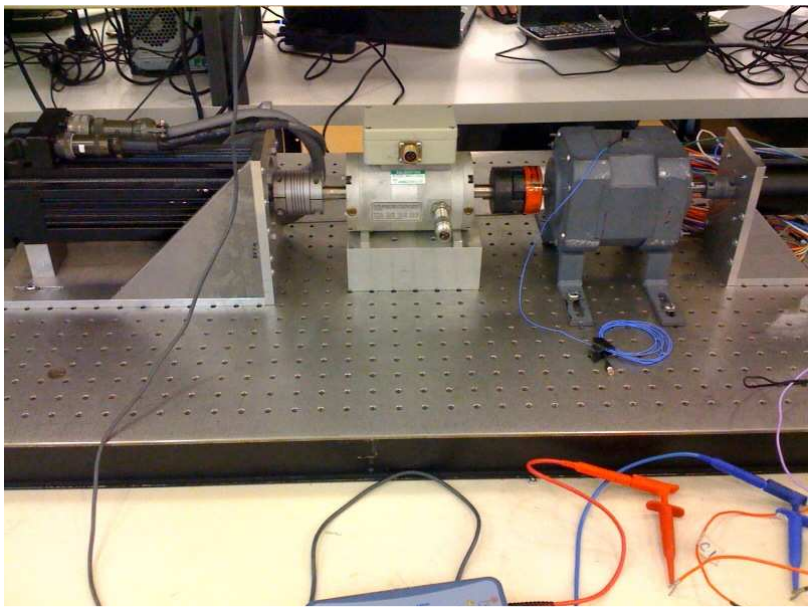

Experimental setup

REFERENCES

1. P. C. Krause, O. Wasynczuk, and S. D. Sudhoff, “Analysis of Electric Machinery and Drive Systems”, 2nd ed., John Wiley and Sons, Piscataway, N.J., pp. 191-274, 2002.
2. I. Takahashi, and T. Noguchi,“A New Quick-Response and High-Efficiency Control Strategy of an Induction Motor”, IEEE Transactions on Industrial Applications, Vol. IA-22, No. 5, pp. 495-502, 1986.
3. T. M. Jahns and W. L. Soong, “Pulsating torque minimization techniques for permanent magnet ac drives- A review”, IEEE Transactions on Industrial Electronics, vol. 43, pp. 321–330, Apr. 1996.
4. C. Studer, A. Keyhani, T. Sebastian, and S. K. Murthy, “Study of cogging torque in permanent magnet machines”, in Proc. IEEE 32nd Ind. Applications Soc. (IAS) Annual Meeting, vol. 1, Oct. 1997, pp. 42–49.
5. D. C. Hanselman, “Effect of skew, pole count and slot count on brushless motor radial force, cogging torque and back EMF,” Inst. Elect. Eng. Proc.—Elect. Power Appl., vol. 144, no. 5, pp. 325–330, Sep. 1997.
6. J. Y. Hung and Z. Ding, “Design of currents to reduce torque ripple in brushless permanent magnet motors”, Proc. Inst. Elect. Eng. B, vol. 140, no. 4, pp. 260-266, 1993.
7. D. C. Hanselman, “Minimum torque ripple, maximum efficiency excitation of brushless permanent magnet motors”, IEEE Transactions on Ind. Electronics, vol. 41, pp. 292–300, June 1994.
8. V. Petrovic, R. Ortega, A. M. Stankovic, and G. Tadmor, “Design and implementation of an adaptive controller for torque ripple minimization in PM synchronous motors”, IEEE Transactions on Power Electronics, vol. 15, pp. 871– 880, Sept. 2000.
9. T. S. Low, T. H. Lee, K. J. Tseng, and K. S. Lock, “Servo performance of A BLDC drive with instantaneous torque control”, IEEE Transactions on Industrial Applications, vol. 28, pp. 455–462, Apr. 1992.
10. N. Matsui, T. Makino, and H. Satoh, “Auto-compensation of torque ripple of direct drive motor by torque observer”, IEEE Transactions on Industrial Applications, vol. 29, pp. 187–194, Feb. 1993.
11. S. K. Chung, H. S. Kim, C. G. Kim, and M.-J. Youn, “A new instantaneous torque control of PM synchronous motor for high-performance directdrive applications”, IEEE Transactions on Power Electronics, vol. 13, pp. 388-400, May 1998.

12. F. Colamartino, C. Marchand, and A. Razek, “Torque ripple minimization in permanent magnet synchronous servo drive,” IEEE Transactions on Energy Conversion, vol. 14, pp. 616–621, Sept. 1999.

13. Q. Weizhe, S. K Panda, J. X. Xu, “Torque ripple minimization in PM synchronous motors using iterative learning control”**,** IEEE Transactions on Power Electronics, Volume 19, Issue 2, March 2004, pp. 272 – 279. 116

14. P. Zheng, J. Zhao, J. Han, J. Wang, Z. Yao, and R. Liu, “Optimization of the Magnetic Pole Shape of a Permanent-Magnet Synchronous Motor”, IEEE Transactions on Magnetics, Volume 43, Issue 6, June 2007, pp. 2531 – 2533.

15. A. Kioumarsi, M. Moallem, and B. Fahimi, “Mitigation of Torque Ripple in Interior Permanent Magnet Motors by Optimal Shape Design” IEEE Transactions on Magnetics, Volume 42, Issue 11, Nov. 2006, pp. 3706 – 3711.

16. J. Piotrowski, “Shaft Alignment Handbook”, New York: Marcel Dekker, 1995.

17. K. Komeza, A. Pelikant, J. Tegopoulos, S. Wiak, “Comparative computation of forces and torques of electromagnetic devices by means of different formulae”, IEEE Transactions on Magnetics, Volume 30, Issue 5, Part 2, Sep 1994, pp. 3475 – 3478.

18. W. Muller, “Comparison of different methods of force calculation”, IEEE Transactions on Magnetics, Vol. 26, No. 2, Mar 1990, pp. 1058-1061.

19. J. Mizia, K. Adamiak, A. R. Eastham, and G. E. Dawson, “Finite element force calculation: comparison of methods for electric machines”, IEEE Transactions on Magnetics, Vol. 24, Issue 1, Jan. 1988, pp.447 – 450.

20. W. Zhu, B. Fahimi, and S. Pekarek, “A Field Reconstruction Method for Optimal Excitation of Permanent Magnet Synchronous Machines”, IEEE Transactions on Energy Conversion, Vol.2, 2006.

21. A. Khoobroo, B. Fahimi, S. Pekarek, “A new field reconstruction method for permanent magnet synchronous machines”, IECON Int. Conf. on Ind. Electron. pp. 2009 – 2013, Nov 2008.

22. J. R. Melcher, Continuum Electromechanics, MIT Press, 1981.

23. A. B. Proca, A. Keyhani, A. El-Antably, W. Lu, and M. Dai, “Analytical model for permanent magnet motors with surface mounted magnets”, IEEE Transaction on Energy Conversion, Volume 18, Issue 3, pp. 386–391, Sept. 2003.

24. Leonhard, W., Control of Electrical Drives, 3rd ed., Springler-Verlag, Berlin Heidelberg, pp. 12, 155-253, 2001

25. J. Holtz and L. Springob, “Identification and compensation of torque ripple in high precision permanent magnet motor drives," IEEE Transactions Ind. Application., vol. 43, no. 2, pp. 309-320, Feb. 1996.

26. V. Petrović, R. Ortega, A. M. Stanković, and G. Tadmor, “Design and implementation of an adaptive controller for torque ripple minimization in PM synchronous motors," IEEE Transactions on Power Electronics, vol. 15, no. 5, pp. 871 - 880, Sept. 2000.

BIOGRAPHICAL INFORMATION

Banharn Sutthiphornsombat was born on November 2, 1978 in Bangkok, Thailand. He received his Bachelor of Science in Electrical Engineering from King Mongkut's Institute of Technology North Bangkok, Thailand, and Master of Engineering in Electrical Engineering from King Mongkut's University of Technology Thonburi. His research interests include DC-DC converters, electrical motor drives, power electronics, and renewable energy.